

Université de Montréal

**Dynamique et ergodicité des chaînes de spins
quantiques critiques de Fredkin et Ising–Kawasaki**

par

Gabriel Longpré

Département de physique
Faculté des arts et des sciences

Mémoire présenté à la Faculté des études supérieures et postdoctorales
en vue de l'obtention du grade de
Maître ès sciences (M.Sc.)
en Physique

15 décembre 2021

Université de Montréal

Faculté des arts et des sciences

Ce mémoire intitulé

**Dynamique et ergodicité des chaînes de spins
quantiques critiques de Fredkin et Ising–Kawasaki**

présenté par

Gabriel Longpré

a été évalué par un jury composé des personnes suivantes :

Normand Mousseau

(président-rapporteur)

William Witczak-Krempa

(directeur de recherche)

Yvan Saint-Aubin

(membre du jury)

Mémoire accepté le :

Résumé

Ce mémoire est composé de deux articles portant respectivement sur les chaînes de spin- $1/2$ critiques quantiques d’Ising–Kawasaki et de Fredkin. La première chaîne provient d’une chaîne d’Ising classique couplée à un bain thermique par une dynamique de Kawasaki. La deuxième chaîne est une généralisation de la chaîne fortement intriquée de Motzkin. Les deux chaînes sont étudiées avec des conditions frontière périodiques. L’objectif principal est de caractériser la dynamique de ces deux chaînes. D’abord, les exposants critiques dynamiques obtenus suggèrent que, à basse énergie, les deux systèmes comportent de multiples dynamiques. Dans les secteurs à un et deux magnons, nous obtenons un exposant $z = 2$ pour les deux chaînes. Pour la chaîne d’Ising–Kawasaki, à fort couplage, l’exposant dynamique global est plutôt $z = 3$. Pour la chaîne de Fredkin, l’exposant dépend de la parité de la longueur de la chaîne. Nous obtenons $z = 3.23 \pm 0.20$ dans le cas pair et $z = 2.71 \pm 0.09$ dans le cas impair. Ensuite, les symétries des systèmes permettent d’obtenir les états propres comme solutions d’ondes de spin dans les secteurs à un et deux magnons. Ces solutions sont présentées pour les deux chaînes et nous étudions leurs continuums de dispersion. Cependant, l’étude de la statistique des niveaux d’énergie indique que de telles solutions ne peuvent être obtenues dans les secteurs de polarisation plus basse. En effet, la distribution des espacements des niveaux d’énergie normalisés dans les secteurs faiblement polarisés correspond à une distribution de Wigner. Selon la conjecture de Berry-Tabor, cela indique que les deux systèmes ne sont pas intégrables. Finalement, pour la chaîne de Fredkin, nous étudions la dispersion des états faiblement excités. Cette dispersion est anomale puisqu’elle dépend de la longueur de la chaîne. En combinant le facteur d’échelle de l’amplitude des branches avec l’exposant dynamique à impulsion fixée, on trouve un exposant dynamique critique $z = 2.8$.

Mots-clés : Chaînes de spin- $1/2$ quantiques critiques, Ising–Kawasaki, Fredkin, statistique des niveaux d’énergie, intégrabilité, ergodicité, exposant dynamique critique, dispersion, solutions d’ondes de spin.

Abstract

This thesis is composed of two scientific articles studying respectively the critical quantum spin-1/2 chains of Ising–Kawasaki and Fredkin. The first chain comes from a classical Ising chain coupled to a thermal bath via the Kawasaki dynamic. The second chain is a generalization of the strongly entangled Motzkin chain. The two chains are studied with periodic boundary conditions. The main objective is to characterize the dynamics of these two chains. First, the dynamical critical exponents obtained suggest that, at low energy, the two systems host multiple dynamics. In the one and two magnon sectors, we get an exponent $z = 2$ for the two chains. For the Ising–Kawasaki chain, at strong coupling, the global dynamical exponent is rather $z = 3$. For the Fredkin chain, the exponent depends on the parity of the length of the chain. We get $z = 3.23 \pm 0.20$ in the even case and $z = 2.71 \pm 0.09$ in the odd case. Afterwards, the symmetries of the systems make it possible to obtain the eigenstates as spin wave solutions in the one- and two-magnon sectors. These solutions are presented for the two chains and their dispersion continua is studied. However, the study of the statistics of energy levels indicates that such solutions cannot be obtained in lower polarization sectors. Indeed, the distribution of the spacings of the normalized energy levels in the weakly polarized sectors corresponds to a Wigner distribution. According to the Berry-Tabor conjecture, this indicates that the two systems are not integrable. Finally, for the Fredkin chain, we study the dispersion of weakly excited states. This dispersion is anomalous since it depends on the length of the chain. By combining the branch amplitude scaling with the fixed momentum dynamic exponent, we find a dynamical critical exponent $z = 2.8$.

Keywords : Critical quantum spin-1/2 chains, Ising–Kawasaki, Fredkin, energy level statistics, integrability, ergodicity, dynamical critical exponent, dispersion, spin-wave solutions.

Table des matières

Résumé	3
Abstract	4
Liste des figures	7
Liste des sigles et des abréviations	8
Remerciements	9
Introduction	10
Ising–Kawasaki	10
Fredkin	11
Statistique des niveaux d'énergie	12
Contributions de l'auteur	13
Article 1. Excitations and ergodicity of critical quantum spin chains from non-equilibrium classical dynamics	14
1.1. Introduction	14
1.2. The Model	16
1.2.1. Ground states	18
1.3. Spin wave solutions	19
1.3.1. One-magnon sector	19
1.3.2. Two-magnon sector	20
1.3.2.1. Ferromagnetic $J > 0$	22
1.3.2.2. Antiferromagnetic $J < 0$	23
1.3.3. Dynamical critical exponents	25
1.4. Energy Level Statistics	26
1.5. Conclusion	28

Acknowledgements	29
Article 2. Dynamics of periodic Fredkin spin chains	31
2.1. Introduction	31
2.2. Fredkin Spin Chain	32
2.2.1. Ground States	33
2.3. Dynamical exponents	34
2.4. Spin wave solutions	35
2.5. Dispersion	37
2.6. Energy Level Statistics	38
2.7. Conclusion	39
Acknowledgements	41
Conclusion	42
Références bibliographiques	44
Annexe A. Annexe de l'article 1	49
A.1. Two-magnon continuum at large $ \kappa $	49
A.2. Bloch basis	49
A.3. Numerical study of energy level spacings	50
A.4. Finite-size scaling	51
Annexe B. Annexe de l'article 2	52
B.1. Finite-size effects on the dynamical exponents	52
B.2. Finite-size effects on the dispersion	52

Liste des figures

1.1	Continuums de dispersion de la chaîne d’Ising–Kawasaki pour $\kappa = 0$ et 0.5	22
1.2	Continuums de dispersion de la chaîne d’Ising–Kawasaki près de la transition à $\kappa = \kappa_x$	24
1.3	Continuums de dispersion de la chaîne d’Ising–Kawasaki pour $\kappa = -0.6$	25
1.4	Dépendance des facteurs des équations de Bethe pour le plus proche voisin et le suivant sur κ	25
1.5	Statistique des niveaux d’énergie pour un secteur de symétrie de la chaîne d’Ising–Kawasaki.....	27
1.6	Statistique des niveaux d’énergie pour deux secteurs de symétrie de la chaîne d’Ising–Kawasaki.....	28
1.7	Coefficient α dans chaque secteur de symétrie de la chaîne d’Ising–Kawasaki.....	29
2.1	Croissance d’échelle de l’écart d’énergie de la première excitation de la chaîne de Fredkin.....	34
2.2	Croissance d’échelle de l’écart d’énergie de la première excitation à basse impulsion de la chaîne de Fredkin.....	35
2.3	Continuums de dispersion de la chaîne de Fredkin dans le secteur à deux magnons.	37
2.4	Continuums de dispersion à basse énergie dans les secteurs faiblement polarisés de la chaîne de Fredkin.....	38
2.5	Statistique des niveaux d’énergie pour un secteur de symétrie de la chaîne de Fredkin.....	40
2.6	Coefficient α dans chaque secteur de symétrie de la chaîne de Fredkin.....	40
A.1	Continuums de dispersion de la chaîne d’Ising–Kawasaki pour $\kappa = \pm\infty$	50
A.2	Dépendance du coefficient α sur la longueur de la chaîne d’Ising–Kawasaki.	51
B.1	Dépendance des paramètres de dispersion sur la longueur de la chaîne de Fredkin.	52

Liste des sigles et des abréviations

CDP	Propriété de décomposition en agrégats, de l'anglais <i>Cluster decomposition property</i> ;
DMRG	Groupe de renormalisation de matrice de densité, de l'anglais <i>Density matrix renormalization group</i> ;
ELS	Statistiques de niveau d'énergie, de l'anglais <i>Energy level statistics</i> ;
NN	Voisin le plus proche, de l'anglais <i>Nearest Neighbor</i> ;
NNN	Second voisin le plus proche, de l'anglais <i>Next Nearest Neighbor</i> ;
PBC	Conditions frontière périodiques, de l'anglais <i>Periodic boundary conditions</i> ;
RMT	Théorie des matrices aléatoires, de l'anglais <i>Random matrix theory</i> .

Remerciements

Je souhaite d'abord remercier Stéphane Vinet pour sa collaboration, son aide et son soutien. Même si nous travaillions sur les mêmes modèles, je n'ai jamais senti de compétition. Ce fut très agréable d'avoir quelqu'un à qui on peut poser toutes ses questions, aussi stupides soit-elles, sans honte ni appréhension de jugement. De la même façon, ce fut très agréable et gratifiant de pouvoir répondre aux tiennes.

Merci à mon directeur de recherche, William Witczak-Krempa, de m'avoir proposé un projet de recherche qui correspond à mes intérêts et de m'avoir guidé dans ce projet.

Je suis très reconnaissant du soutien moral de ma conjointe, merci de m'encourager, de m'écouter et de me rappeler de respecter mes limites. Merci également à mes parents pour leur support inconditionnel. Merci aussi à mon professeur de piano de m'avoir permis de m'évader dans la musique.

J'aimerais également remercier mes amis et collègues, Lucie Maude Fournier, Juliette Geoffrion, Mélina Riuz, Simon Garneau-Desroches, Simon Martin et Louis Godbout. Merci d'avoir égayé la vie au bureau et merci d'encourager l'entraide. Je n'aurais d'ailleurs probablement pas choisi ce groupe de recherche sans la présence d'Éric Dupuis, merci pour ta gentillesse ineffable. Merci également à Gilles Perez pour tes conseils pendant la rédaction du deuxième article.

Merci à Olivier Gingras, Félix Antoine Goudreault, Vincent Binet pour leur aide avec les grappes de Calcul Canada et l'installation de divers logiciels et librairies. Merci à Sophie Tremblay de toujours être là pour aider les étudiant.e.s, et de le faire avec enthousiasme.

Merci au Conseil de recherches en sciences naturelles et en génie du Canada, au Fonds de recherche du Québec – Nature et technologie, et au Collège de Bois-de-Boulogne pour le soutien financier.

Introduction

Les modèles de spin quantiques permettent d'expliquer le comportement magnétique des matériaux. Ils ont l'avantage d'être assez simples conceptuellement, mais de quand même renfermer plusieurs phénomènes physiques riches et complexes. C'est particulièrement le cas des modèles unidimensionnels, les chaînes de spin, pour lesquels des solutions exactes peuvent parfois être trouvées. Ces modèles permettent entre autres une meilleure compréhension des transitions de phase quantique, de l'intrication et de la dispersion dans les matériaux. [1]

Dans ce mémoire les chaînes de spin d'Ising–Kawasaki et de Fredkin seront étudiées. Ce sont des chaînes de spin-1/2 critiques quantiques pour lesquelles l'écart d'énergie de la première excitation s'affaisse dans la limite thermodynamique.

Ising–Kawasaki

La dynamique de la chaîne quantique d'Ising–Kawasaki provient d'un système classique. En effet, la dynamique de plusieurs systèmes classiques hors d'équilibre peut être reliée à celle d'un système quantique fermé [2, 3]. À cette fin, l'équation de Markov du système classique est interprétée comme une équation de Schrödinger en temps imaginaire. L'Hamiltonien obtenu correspond alors à l'opérateur de translation temporelle sur l'espace de Fock de la chaîne de Markov [4, 5]. Aussi, l'exposant de la croissance d'échelle de la longueur de corrélation du système classique correspond alors à l'exposant dynamique du système quantique. Cet exposant est caractéristique de la classe d'universalité de laquelle le système provient [6, 7]. Ainsi, on peut utiliser les outils de la mécanique quantique, tel que l'ansatz de Bethe et la DMRG, afin d'étudier les processus classiques stochastiques hors d'équilibre. Dans le cas de la chaîne d'Ising–Kawasaki, le système classique correspondant est une chaîne d'Ising de constante J couplée à un bain thermique de température T par une dynamique de Kawasaki. Le modèle d'Ising n'a pas de dynamique intrinsèque. Ainsi, une dynamique de Kawasaki qui décrit une interaction d'échange d'états locaux y est introduite. Elle interchange des paires de spins voisins antiparallèles et préserve donc l'aimantation [8]. Le taux de transition des échanges dépend de la variation de l'énergie d'Ising qu'ils produisent.

L'Hamiltonien du système quantique est

$$H_{\text{Ising-Kawasaki}} = \gamma_\kappa \sum_{i=1}^N \left(1 + \delta_\kappa \sigma_i^z \sigma_{i-1}^z \sigma_{i+2}^z \right) \left(\sigma_i^x \sigma_{i+1}^x + \sigma_i^y \sigma_{i+1}^y \right) \\ + \frac{1}{4} \sum_{i=1}^N \left[1 + \alpha_\kappa \sigma_i^z \sigma_{i+2}^z - (1 + \alpha_\kappa) \sigma_i^z \sigma_{i+1}^z \right],$$

où $\kappa = J/(k_B T)$, $\gamma_\kappa = -\frac{1}{8}(1 + \operatorname{sech}(2\kappa))$, $\delta_\kappa = \tanh(\kappa)^2$ et $\alpha_\kappa = \tanh(2\kappa)$. La dérivation de l'Hamiltonien est décrite dans l'article [9] et dans la section 1.2. Dans son article, Grynberg étudie l'exposant dynamique critique pour des conditions frontière périodiques. Il s'intéresse à la limite $\kappa \rightarrow \infty$, qui correspond à la limite à basse température et fort couplage dans la chaîne classique, et y obtient $z \approx 3.1$, ce qui est cohérent avec l'exposant dominant $z = 3$ dans les secteurs faiblement polarisés [10, 11, 12, 13]. Cette valeur correspond à une dynamique sous-diffusive due au ralentissement de la relaxation par la contrainte de conservation de l'aimantation [14]. Cette valeur contraste également avec l'exposant dynamique diffusif $z = 2$ dans l'autre limite $\kappa \rightarrow 0$ qui correspond à la chaîne XXX d'Heisenberg. Cet autre exposant est retrouvé pour toutes valeurs de κ dans les secteurs à un et deux magnons.

Fredkin

La chaîne de Fredkin est obtenue comme une généralisation aux spins demi-entiers de la chaîne de Motzkin [15, 16]. La chaîne de Fredkin peut également être exprimée en termes de portes logiques CSWAP, aussi nommées portes de Fredkin. Comme la chaîne d'Ising-Kawasaki, elle préserve l'aimantation. En représentant les états produits par des parenthèses ouvrantes et fermantes : $|\uparrow\rangle \mapsto |()\rangle$ et $|\downarrow\rangle \mapsto |)\rangle$, il est possible de décrire l'interaction comme le déplacement de paires () le long de la chaîne :

$$() \leftrightarrow)() \quad ((\leftrightarrow ()().$$

L'Hamiltonien du système est

$$H_{\text{Fredkin}} = \sum_{i=1}^N (1 + \sigma_i^z)(1 - \vec{\sigma}_{i+1} \cdot \vec{\sigma}_{i+2}) + (1 - \vec{\sigma}_i \cdot \vec{\sigma}_{i+1})(1 - \sigma_{i+2}^z).$$

Ainsi, comme pour la chaîne d'Ising-Kawasaki, cette interaction préserve l'aimantation. Elle préserve également le nombre de parenthèses ouvrantes et fermantes orphelines. Pour des conditions frontière non périodiques, cette symétrie sépare la base des états produits en classes d'équivalence $C_{a,b}(N)$ où a et b sont respectivement le nombre de parenthèses fermantes et ouvrantes orphelines des états produits à N sites. La quasi-totalité des résultats sur cette chaîne utilise une condition frontière fixée donnée par l'ajout du terme $H_\partial = |\downarrow_1\rangle \langle \downarrow_1| + |\uparrow_N\rangle \langle \uparrow_N|$ qui permet d'obtenir un état fondamental unique donné par

la somme symétrique des mots de Dyck [15, 17, 18, 19, 20, 21, 22, 23]. Cette non-dégénérescence permet de vérifier la CDP puisqu'elle est trivialement brisée pour des états dégénérés. Cette propriété stipule que les fonctions de corrélation à deux points tendent vers zéro lorsque les deux points s'éloignent [23]. Elle explique pourquoi les parties éloignées d'un système se comportent de façon indépendante. On s'attend à ce qu'elle soit respectée pour les systèmes à interactions locales, comme les chaînes d'Ising–Kawasaki, de Fredkin et de Motzkin. Cependant, elle n'est pas respectée par ces deux dernières [17]. En effet, les chaînes de Fredkin et Motzkin présentent des niveaux élevés d'intrication [24, 25, 22]. Elles transgressent la loi du périmètre par un facteur logarithmique, c'est-à-dire que l'entropie d'intrication croît avec le logarithme de la taille de la sous-région. La loi du périmètre devrait être respectée pour les systèmes avec une bande d'énergie interdite et transgressee d'au plus un facteur logarithmique pour les systèmes critiques [24, 26, 27]. Plusieurs articles étudient également la dynamique de la chaîne de Fredkin. Comme la chaîne d'Ising–Kawasaki, le système comporte plusieurs dynamiques et des exposants sous-diffusifs près de $z = 3$ [19, 17, 28]. Ces résultats utilisent la condition frontière mentionnée précédemment. La section 2.3 présente les résultats obtenus pour des conditions frontière périodiques.

Statistique des niveaux d'énergie

Selon une conjecture de Percival [29], les spectres des systèmes fermés dans la limite semi-classique se séparent en deux classes : réguliers et irréguliers. La première se présente dans les systèmes intégrables, c'est-à-dire dans les systèmes où le nombre de constantes du mouvement est égal au nombre de degrés de liberté. La deuxième se présente dans les systèmes non intégrables, où le nombre de symétries ne permet pas une classification unique par les nombres quantiques. Fondée sur cette conjecture et sur des résultats équivalents en RMT, la conjecture de Berry-Tabor [30] stipule que les spectres réguliers des systèmes quantiques intégrables sont caractérisés par des niveaux d'énergie décorrélés avec une forte agrégation. Par contre, si le spectre est séparé en secteurs de symétrie, en considérant uniquement les énergies des états de mêmes nombres quantiques, une corrélation et une forte répulsion des niveaux d'énergie adjacents sont observées. Dans le contexte de la conjecture de Berry-Tabor et des chaînes de spin, l'intégrabilité signifie qu'une solution complète peut être obtenue par l'ansatz de Bethe coordonnée [31].

La conjecture indique également que la statistique des niveaux d'énergie du spectre *déplié* devrait prendre une forme caractéristique selon la classe du spectre. Le spectre doit être *déplié* afin d'en extraire les caractéristiques universelles. Le spectre *déplié* correspond aux énergies renormalisées de façon à ce que la densité d'états locale soit constante et égale à un partout dans le spectre. Cela retire la variation à grande échelle, adimensionne le spectre et permet l'utilisation des résultats universels et adimensionnels de la RMT. Ainsi, si, par exemple, une transformation linéaire est appliquée sur l'Hamiltonien, son spectre

déplié restera inchangé. Il existe plusieurs techniques pour *déplier* le spectre et la notion de variation à grande échelle n'a pas de définition mathématique rigoureuse dans ce contexte. Il est donc important de vérifier que la technique utilisée fonctionne adéquatement pour le système étudié. [32, 33, 34, 35, 36]

La distribution de l'espacement des niveaux d'énergie $P(s)$ correspond à la probabilité que deux énergies adjacentes du spectre *déplié* aient un espacement s . Pour le spectre d'un système intégrable ou un spectre qui n'est pas séparé en secteurs de symétrie, cette distribution serait une distribution exponentielle d'espérance $\lambda = 1$, décrivant un processus de Poisson et un spectre sans répulsion. Pour le spectre d'un système non intégrable, ou d'un spectre séparé en secteurs de symétrie pour toutes ses symétries, cette distribution serait une distribution de Wigner correspondant à l'ensemble orthogonal gaussien et à un spectre avec répulsion. La méthode présentée dans les articles de Kudo et Deguchi [35, 36] sera suivie dans les sections 1.4 et 2.6 afin d'obtenir le spectre *déplié* pour déterminer la non-intégrabilité des chaînes d'Ising–Kawasaki et de Fredkin.

Contributions de l'auteur

Les auteurs des deux articles sont Gabriel Longpré (GL), Stéphane Vinet (SV) et William Witczak-Krempa (WWK).

Dans l'article 1, GL a rédigé les sections 1.4, 1.6.2, 1.6.3 et 1.6.4. Il a également participé à la rédaction de la section 1.2 avec SV. Il a obtenu les états fondamentaux présentés à la section 1.2.1. Les statistiques de niveaux d'énergie de la section 1.4 ont été calculées et analysées par GL. SV a rédigé les sections 1.3 et 1.6.1 et a obtenu la dérivation de l'Hamiltonien présentée à la section 1.2. Les solutions d'ondes de spin de la section 1.3 ont été obtenues par SV.

Dans l'article 2, GL a rédigé les sections 2.2, 2.3, 2.5, 2.6 et 2.8. Il a également obtenu les résultats présentés dans ces sections. La section 2.4 a été corédigée avec SV qui a obtenu les résultats de cette section. La section 2.7 a été corédigée avec WWK.

Dans les deux articles, WWK a rédigé le résumé, l'introduction, la conclusion et a travaillé sur toutes les autres sections. Il a été l'architecte des projets et a dirigé l'ensemble de la recherche présentée. Les trois auteurs ont participé à la révision des deux articles en entier.

Article 1

Excitations and ergodicity of critical quantum spin chains from non-equilibrium classical dynamics

Par Stéphane Vinet, Gabriel Longpré et William Witczak-Krempa.

Accepté dans *SciPost Physics Core* le 5 avril 2022.

ArXiv e-print : <https://arxiv.org/abs/2107.04615v3>

Abstract. We study a quantum spin-1/2 chain that is dual to the canonical problem of non-equilibrium Kawasaki dynamics of a classical Ising chain coupled to a thermal bath. The Hamiltonian is obtained for the general disordered case with non-uniform Ising couplings. The quantum spin chain (dubbed Ising-Kawasaki) is stoquastic, and depends on the Ising couplings normalized by the bath's temperature. We give its exact ground states. Proceeding with uniform couplings, we study the one- and two-magnon excitations. Solutions for the latter are derived via a Bethe Ansatz scheme. In the antiferromagnetic regime, the two-magnon branch states show intricate behavior, especially regarding their hybridization with the continuum. We find that the gapless chain hosts multiple dynamics at low energy as seen through the presence of multiple dynamical critical exponents. Finally, we analyze the full energy level spacing distribution as a function of the Ising coupling. We conclude that the system is non-integrable for generic parameters, or equivalently, that the corresponding non-equilibrium classical dynamics are ergodic.

1.1. Introduction

The exact correspondance between the non-equilibrium dynamics of certain classical systems and the dynamics of closed quantum systems has a rich history [4]. This classical-quantum duality follows from the fact that the Markov or Master equation can be mapped to a quantum Schrödinger equation in imaginary time. One can thus gain insights about the dynamics from either side of the correspondance. This has been used in the study of

various systems, such as the non-equilibrium dynamics of particles or spins on the lattice, and, on the quantum side of the mapping, various quantum spin Hamiltonians including Heisenberg and XY models, as well as dimer models [2, 37, 3, 4, 9, 38, 39]. One powerful application has been to use the integrability of certain quantum spin chains to solve the corresponding non-equilibrium classical dynamics [4]. Alternatively, one can generate new quantum Hamiltonians starting from classical dynamical models. This is the approach that we shall take in this work.

Our analysis begins with a canonical problem in non-equilibrium statistical mechanics: the non-equilibrium dynamics of a 1d classical Ising spin chain subject to Kawasaki (spin-preserving) dynamics. More precisely, the Ising chain couples to a thermal bath that allows anti-aligned neighboring spins to exchange positions. The corresponding quantum Hamiltonian is a spin-1/2 chain with a global U(1) symmetry, and contains up to 4-spin interactions. We shall refer to it as the *quantum Ising-Kawasaki chain*. In the limit of uniform Ising couplings (we also discuss the non uniform case), the quantum spin chain depends on a single parameter: βJ , the Ising coupling normalized by the temperature of the classical bath, $1/\beta$. This temperature does not correspond to a temperature in the quantum system, instead it simply determines the coupling of the quantum spin chain. The latter is studied as a closed quantum system evolving under unitary Hamiltonian evolution. The exact groundstates are simply obtained from the Boltzmann distribution of the classical Ising model; the groundstate degeneracy is $N + 1$ corresponding to the different magnetization sectors for a chain of N sites. The 1-magnon excitations (where 1 spin is flipped in a ferromagnetic sea) are obtained exactly, and disperse quadratically at low wavevectors. Combined with the analysis from previous works [40, 10, 11, 12, 13, 41, 42, 43], this leads us to conclude that the quantum spin chain, and corresponding non-equilibrium dynamics, host multiple dynamical critical exponents, one of them being $z = 2$. Next, we derive solutions for the two-magnon spectra via a Bethe Ansatz scheme. In the antiferromagnetic regime, the 2-magnon branch states show intricate behavior, especially regarding hybridization with the continuum. Next, we turn to the study of the entire eigenspectrum, and numerically analyze the energy level statistics using exact diagonalization on short chains, $N \leq 25$. We conclude that the system is non-integrable for generic values of βJ , or equivalently, that the corresponding non-equilibrium classical dynamics are ergodic as expected.

Interestingly, the quantum Ising-Kawasaki chain shows phenomena that are similar to certain frustration free quantum spin chains that were recently introduced with motivation from a quantum information perspective: the Motzkin [44, 45] and Fredkin [46] spin chains. Just like the Ising-Kawasaki chain, these gapless chains show multiple dynamics at low energy [47, 19]. Besides the rich dynamical and entanglement properties of these chains, it has been shown that the Motzkin chain realizes a local approximate quantum error correcting

code in its ground space [48]. It would be interesting to study the Kawasaki chain from such a quantum information perspective.

The rest of the paper is organized as follows. In Section 1.2 we introduce the classical non-equilibrium model, and the resulting quantum Hamiltonian. We give its exact groundstates. In Section 1.3, turning to the uniform case, we find the 1- and 2-magnon excitations via the standard Bethe Ansatz. Among others, we show exactly that the dynamical critical exponent in those sectors is $z = 2$. In Section 1.4, we use exact diagonalization to determine the energy level spacing distribution for the entire spectrum. Our analysis shows that the system is non-integrable for generic βJ , which in turn implies that the classical Kawasaki dynamics are ergodic. We give a summary of our results and various extensions in Section 1.5.

1.2. The Model

As the Ising model is a static model in equilibrium, dynamical generalizations have been introduced notably by Glauber and Kawasaki [49, 8] in order to study relaxational processes near equilibrium. Glauber dynamics consists of single spin-flip processes while Kawasaki proposes a spin exchange for a pair of unequal spins. Kawasaki dynamics thus conserves the total magnetization. The quantum Kawasaki spin chain is obtained from the corresponding Markov operator [9], as we now discuss.

For a classical Ising chain of length N , a state is identified by a vector $\vec{s} \in \{-1,1\}^N$. We generalize the analysis of [2, 9] by working with non uniform couplings, for which the Ising energy reads

$$E_I(\vec{s}) = - \sum_{i=1}^N J_i s_i s_{i+1}, \quad (1.2.1)$$

where the coupling constant J_i is positive/negative for ferromagnetic/antiferromagnetic interactions. Assuming periodic boundary conditions, we have that $s_{N+1} = s_1$. In thermal equilibrium, the probability to find a state is given by its Boltzmann weight $P(\vec{s}) = e^{-\beta E_I(\vec{s})}/Z$, where $\beta = 1/(k_B T)$ is the inverse temperature of the heat bath and Z is the canonical partition function. After endowing the system with Kawasaki *non-equilibrium* dynamics, the evolution of the probability obeys the gain-loss equation:

$$\partial_t P(\vec{s},t) = \sum_{\vec{s}' \in \{-1,1\}^N} [W(\vec{s}' \rightarrow \vec{s})P(\vec{s}',t) - W(\vec{s} \rightarrow \vec{s}')P(\vec{s},t)], \quad (1.2.2)$$

which describes the evolution of the probability $P(\vec{s},t)$ that the system will be in the state \vec{s} at time t . In order to derive all subsequent probability distributions from the action of an evolution operator on a given initial distribution, Eq. (1.2.2) can be viewed as the Schrödinger evolution in imaginary time of a pseudo-Hamiltonian such that $\partial_t |P(t)\rangle = -\hat{W}|P(t)\rangle$. Consequently, $|P(t)\rangle = e^{-\hat{W}t}|P(0)\rangle$, where $\hat{W} = \hat{W}_d + \hat{W}_{nd}$ whose diagonal and

non-diagonal matrix entries are

$$\langle \vec{s} | \hat{W}_d | \vec{s} \rangle = \sum_{\vec{s}' \neq \vec{s}} W(\vec{s}' \rightarrow \vec{s}) \quad \text{and} \quad \langle \vec{s}' | \hat{W}_{nd} | \vec{s} \rangle = -W(\vec{s} \rightarrow \vec{s}'). \quad (1.2.3)$$

The dimensionless transition probability rate for a state configuration $|\vec{s}\rangle$ to evolve to $|\vec{s}'\rangle$ is taken to be

$$W(\vec{s} \rightarrow \vec{s}') = \frac{1}{2} \left[1 - \tanh \left(\frac{\beta}{2} \Delta E_{\vec{s}, \vec{s}'} \right) \right], \quad (1.2.4)$$

where $|\vec{s}\rangle$ and $|\vec{s}'\rangle$ differ at most by a pair of nearest neighbor spins (NN), and $\Delta E_{\vec{s}, \vec{s}'} = E_I(\vec{s}') - E_I(\vec{s})$ is the Ising energy difference between the two configurations [8]. Using the z -axis in spin space as the quantization axis by promoting s_i variables to Pauli operators σ_i^z , the obtained Markov operator \hat{W} is real but not symmetric. The non-unitary similarity transformation $H' = M\hat{W}M^{-1}$, with

$$M = \exp \left(-\frac{1}{2} \sum_{i=1}^N \kappa_i \sigma_i^z \sigma_{i+1}^z \right), \quad (1.2.5)$$

where $\kappa_i = \beta J_i$, yields a self-adjoint Hamiltonian operator H' . It is important to note that H' and the Markov operator \hat{W} share the same eigenvalues. In addition, an eigenstate $|\psi\rangle$ of H' yields an eigenstate $M|\psi\rangle$ of \hat{W} . Under periodic boundary conditions (PBCs), we find that H' takes the following form:

$$\begin{aligned} H' = & - \sum_{i=1}^N \frac{(\cosh(\kappa_{i+1}) \cosh(\kappa_{i-1}) + \sigma_{i-1}^z \sigma_{i+2}^z \sinh(\kappa_{i+1}) \sinh(\kappa_{i-1}))}{2(\cosh(2\kappa_{i+1}) + \cosh(2\kappa_{i-1}))} (\sigma_i^x \sigma_{i+1}^x + \sigma_i^y \sigma_{i+1}^y) \\ & + \frac{1}{8} \sum_{i=1}^N [2 + (-2 - \tanh(\kappa_i + \kappa_{i-2}) - \tanh(\kappa_i - \kappa_{i-2}) - \tanh(\kappa_{i+2} + \kappa_i) + \tanh(\kappa_{i+2} - \kappa_i)) \sigma_i^z \sigma_{i+1}^z \\ & + (\tanh(\kappa_{i+1} + \kappa_{i-1}) + \tanh(\kappa_{i+1} - \kappa_{i-1}) + \tanh(\kappa_{i+2} + \kappa_i) - \tanh(\kappa_{i+2} - \kappa_i)) \sigma_i^z \sigma_{i+2}^z], \end{aligned} \quad (1.2.6)$$

where the first line generates spin-flips, while the last are diagonal in the σ_i^z basis. We note that in the limit of infinite temperature, $\kappa_i = 0$, we recover the *uniform* ferromagnetic Heisenberg XXX Hamiltonian. This is because the individual values of the couplings J_i become unimportant compared to the large bath temperature $1/\beta$. In that limit, the dynamics simplify, and in fact become integrable. We shall see that this is not the case at finite β .

The Hamiltonian (1.2.6) is *stoquastic* in the standard σ_i^z basis. A Hamiltonian is stoquastic with respect to a given basis if it has only real nonpositive off-diagonal matrix elements in that basis [50]. This can be readily seen from the non-diagonal term of Eq. (1.2.6) as its matrix elements $-\operatorname{sech}(\kappa_{i+1} \pm \kappa_{i-1})/2$ are real and non-positive $\forall \kappa_i$. This implies that its ground states can be expressed as a classical probability distribution [51]. Furthermore, stoquastic Hamiltonians avoid the “sign problem” in quantum Monte Carlo (QMC) algorithms. In particular, the standard quantum-to-classical mapping used in QMC algorithms does

not result in a partition function with Boltzmann weights taking negative or even complex values [52].

For uniform couplings, we find that Eq. (1.2.6) reduces to:

$$H = \gamma_\kappa \sum_{i=1}^N \left(1 + \delta_\kappa \sigma_i^z \sigma_{i-1}^z \sigma_{i+2}^z\right) \left(\sigma_i^x \sigma_{i+1}^x + \sigma_i^y \sigma_{i+1}^y\right) + \frac{1}{4} \sum_{i=1}^N \left[1 + \alpha_\kappa \sigma_i^z \sigma_{i+2}^z - (1 + \alpha_\kappa) \sigma_i^z \sigma_{i+1}^z\right], \quad (1.2.7)$$

where $\gamma_\kappa = -\frac{1}{8}(1 + \text{sech}(2\kappa))$, $\delta_\kappa = \tanh(\kappa)^2$, $\alpha_\kappa = \tanh(2\kappa)$, in agreement with [9].

At $\kappa = \infty$, we obtain $\gamma_\kappa = -1/8$ and $\delta_\kappa = \alpha_\kappa = 1$. The Hamiltonian then takes the form of the folded spin-1/2 XXZ model with an extra diagonal term, as seen for example in [[53]].

1.2.1. Ground states

As the total spin is conserved in the interaction with the thermal bath, the resulting Hamiltonian (1.2.7) conserves total S_T^z (the spin symmetry is enlarged to SU(2) at $\beta = \infty$). We thus have a thermodynamic equilibrium for every spin subsector. The $N + 1$ ground states of the Hamiltonian (1.2.7) are thus obtained by applying the nonunitary similarity transformation (1.2.5) to Ising equilibrium states in each of these subsectors.

At thermodynamic equilibrium, the probability of finding the Ising chain in a configuration \vec{s} is given by the Boltzmann distribution

$$\text{Prob}_{\text{eq}}(\vec{s}) = \frac{1}{Z} \exp(-\beta E_I(\vec{s})) = \frac{1}{Z} \exp\left(\sum_{i=1}^N \kappa_i s_i s_{i+1}\right). \quad (1.2.8)$$

Suppose the total spin $S_T^z = j$ for $j \in \{-N/2, -N/2 + 1, \dots, N/2 - 1, N/2\}$, the Ising thermal equilibrium state for the subsector \mathcal{S}_j can be mapped to the following (not normalized) quantum state

$$|P_{\text{eq},j}\rangle := \sum_{\vec{s} \in \mathcal{S}_j} \text{Prob}_{\text{eq}}(\vec{s}) |\vec{s}\rangle = \frac{1}{Z} \sum_{\vec{s} \in \mathcal{S}_j} \exp(-\beta E_I(\vec{s})) |\vec{s}\rangle, \quad (1.2.9)$$

where $|\vec{s}\rangle$ is labelled by the σ_i^z eigenvalues. The ground state is then obtained by applying the transformation (1.2.5) to $|P_{\text{eq},j}\rangle$, and normalizing the result. Therefore the ground state of H for the subsector of total spin $S_T^z = j$ is

$$|\phi_{0,j}\rangle = \frac{M |P_{\text{eq},j}\rangle}{\langle P_{\text{eq},j} | M M | P_{\text{eq},j} \rangle^{1/2}} = \frac{1}{Z_j^{1/2}} \sum_{\vec{s} \in \mathcal{S}_j} \exp\left(-\frac{\beta}{2} E_I(\vec{s})\right) |\vec{s}\rangle \quad (1.2.10)$$

where $Z_j = \sum_{\vec{s} \in \mathcal{S}_j} \exp(-\beta E_I(\vec{s}))$ is the partition function restricted to the magnetization sector j . Up to an overall constant, each component or amplitude of the groundstate vector (1.2.10) is the square root of the amplitude appearing in the original equilibrium state $|P_{\text{eq},j}\rangle$.

We note that the ground state degeneracy is no longer $N + 1$ at $\beta = \infty$, i.e. as the bath temperature vanishes. The probability rate in Eq. (1.2.4) is zero for transitions that would raise the Ising energy ($\Delta E_{\vec{s},\vec{s}'} > 0$). Consequently, the classical system will often get

stuck in one of the many metastable states for which the only possible transitions would increase the energy. These states correspond to configurations in which each spin kink (domain wall) is separated by more than a nearest-neighbor distance from any other spin kink [40]. The quantum system is further constrained at low temperature by the non-unitary transformation M , which suppresses the energy lowering transitions, and leads to the conservation of the Ising energy $H_{\text{Ising}} = \sum_i \sigma_i^z \sigma_{i+1}^z$, which is directly related to the domain-wall number $n_{\text{dw}} = \frac{1}{2}(N - H_{\text{Ising}})$. This is shown in Appendix A.1. These additional constraints at $\beta = \infty$ give rise to glassy dynamics. We find numerically for the quantum spin chain up to $N = 24$ that the number of ground states $g(N)$ of H at $\kappa = \infty$ is exactly given by

$$g(N) = \left(\frac{1 + \sqrt{5}}{2} \right)^N + |(N - 1 \bmod 6) - 2| + \left\lfloor \frac{N - 2}{3} \right\rfloor \bmod 2, \quad (1.2.11)$$

where $\frac{1 + \sqrt{5}}{2}$ is the golden ratio, and $\lfloor x \rfloor$ corresponds to the floor, i.e. the greatest integer less than or equal to x . Given that Eq. (1.2.11) holds exactly for $N \leq 24$, we expect that it will hold for all N . Consequently, the ground state degeneracy grows exponentially as $(\frac{1 + \sqrt{5}}{2})^N$ at large N , which is in accordance with the scaling of the number of stable configurations for the classical system [40, 54].

1.3. Spin wave solutions

In the remainder of the paper, we shall work with the case of uniform couplings $\kappa_i = \kappa$. The rotational symmetry about the z -axis in spin space implies that the total z -spin $S_T^z = \sum_{i=1}^N \sigma_i^z / 2$ is conserved. Consequently, the Hamiltonian matrix in Eq. (1.2.7) can be block diagonalized according to the total z -spin quantum number $S_T^z \in \{-N/2, -N/2 + 1, \dots, N/2 - 1, N/2\}$. Each of its values corresponds to an eigenspace \mathcal{S}_j of dimension $\binom{N}{N/2 - S_T^z}$. Therefore, the subsectors with $S_T^z = \pm N/2$ consist of a single eigenstate. In section 1.3, we consider the one and two magnon sectors namely $S_T^z = N/2 - 1$ and $S_T^z = N/2 - 2$.

1.3.1. One-magnon sector

For the $S_T^z = N/2 - 1$ sector, the translational symmetry allows for the complete diagonalization of the Hamiltonian. Consequently, the eigenvectors of the translation operator

$$|\psi\rangle = \frac{1}{\sqrt{N}} \sum_{n=1}^N e^{ikn} |n\rangle, \quad (1.3.1)$$

where $|n\rangle$ is the state corresponding to the configuration in which the magnon is in the n^{th} $\in [1, N]$ site, with wavevector $k = 2\pi m/N$ and $m \in [0, N - 1]$, are also eigenvectors of H

whose eigenvalues are given by

$$E_m = 1 - \cos(2\pi m/N). \quad (1.3.2)$$

Setting $m = 0$, one recovers the corresponding ground state from the previous section. Eq. (1.3.1) is the well-studied single-magnon equation of the Heisenberg spin chain studied in [55, 56], among others, with a dynamical critical exponent of $z = 2$ and wavelength $\lambda = 2\pi/k$. Note that Eq. (1.3.2) is independent of κ since the Ising energy does not change as the magnon hops. It can also be seen in the coordinate Bethe ansatz formalism as

$$|\psi\rangle = \sum_{n=1}^N a(n) |n\rangle, \quad (1.3.3)$$

where periodic boundary conditions impose $a(n) = a(n + N)$. The spin-flip component of the Hamiltonian applied onto the state $|n\rangle$ will yield a non-zero result when either $i = n$ or $i + 1 = n$:

$$(\sigma_n^x \sigma_{n+1}^x + \sigma_n^y \sigma_{n+1}^y) |n\rangle = 2 |n+1\rangle, \quad (1.3.4a)$$

$$(\sigma_{n-1}^x \sigma_n^x + \sigma_{n-1}^y \sigma_n^y) |n\rangle = 2 |n-1\rangle. \quad (1.3.4b)$$

evaluating the remaining σ^z terms in the eigenvalue equation $H |\psi\rangle = E |\psi\rangle$ one obtains

$$H \sum_{n=1}^N a(n) |n\rangle = \sum_{n=1}^N a(n) [2\gamma_\kappa(1 + \delta_\kappa)(|n+1\rangle + |n-1\rangle) + |n\rangle], \quad (1.3.5)$$

where $2\gamma_\kappa(1 + \delta_\kappa) = -\frac{1}{4}(1 + \text{sech}(2\kappa))(1 + \tanh(\kappa)^2) = -\frac{1}{2}$ thus the coupling dependence cancels out and we find the following condition for the coefficients $a(n)$:

$$2Ea(n) = 2a(n) - a(n-1) - a(n+1). \quad (1.3.6)$$

Consequently, in accordance with Eq. (1.3.1) we have that $a(n) = e^{ikn}$, as well as N linearly independent solutions of Eq. (1.3.6) obeying periodic boundary conditions for $e^{ik(n+N)} = e^{ikn}$.

1.3.2. Two-magnon sector

Analogously for $S_T^z = N/2 - 2$, we have in the two magnon sector

$$|\psi\rangle = \sum_{1 \leq n_1 < n_2 \leq N}^N a(n_1, n_2) |n_1, n_2\rangle. \quad (1.3.7)$$

We work in the center of mass $K = k_1 + k_2$, with relative coordinate $j = n_2 - n_1$. Based on symmetry considerations, we use the following ansatz for the coefficients $a(n_1, n_2)$:

$$a(n_1, n_2) = e^{iK(n_1+n_2)} g(j), \quad (1.3.8)$$

where $K = m\pi/N$ is the momentum of the center of mass, $m = 0, 1, \dots, N - 1$ and $g(j)$ a function of the number of lattice sites between the two excitations. PBC impose that $a(n_1, n_2) = a(n_2, n_1 + N)$ and so $e^{iKN}g(N - j) = g(j)$. We consequently obtain a periodic condition dependent on the parity of m as in the even case $g(j) = g(N - j)$ whereas in the odd case $g(j) = -g(N - j)$. For even N , these coefficients satisfy the following linear equations given by substituting Eq. (1.3.7) into the Schrödinger equation:

$$Eg(1) = (1 - \alpha_\kappa)g(1) + 4\gamma_\kappa(1 - \delta_\kappa)\cos(K)g(2), \quad (1.3.9)$$

$$Eg(2) = 4\gamma_\kappa(1 - \delta_\kappa)\cos(K)g(1) + (2 + \alpha_\kappa)g(2) - \cos(K)g(3), \quad (1.3.10)$$

$$Eg(j) = -\cos(K)[g(j - 1) + g(j + 1)] + 2g(j), \quad \text{for } 3 \leq j < N/2. \quad (1.3.11)$$

In the limiting case of Eq. (1.3.11) where the magnons are furthest apart $j = n_2 - n_1 = N/2$ we find that $g(j - 1) = e^{im\pi}g(j + 1)$ and so

$$Eg(N/2) = -2\cos(K)g(N/2 - 1) + 2g(N/2), \quad \text{for } m \text{ even}, \quad (1.3.12a)$$

$$Eg(N/2) = 2g(N/2), \quad \text{for } m \text{ odd}. \quad (1.3.12b)$$

For an odd spin chain length the upper bound of j on Eq. (1.3.11) is reduced to $(N - 1)/2$ and Eq. (1.3.12) is changed to

$$Eg\left(\frac{N-1}{2}\right) = -\cos(K)g\left(\frac{N-3}{2}\right) + (2 - \cos(K))g\left(\frac{N-1}{2}\right) \quad \text{for } m \text{ even}, \quad (1.3.13a)$$

$$Eg\left(\frac{N-1}{2}\right) = -\cos(K)g\left(\frac{N-3}{2}\right) + (2 + \cos(K))g\left(\frac{N-1}{2}\right) \quad \text{for } m \text{ odd}. \quad (1.3.13b)$$

One finds that Eq. (1.3.12b) is trivially satisfied by $E = 2$. This result would however yield an overcomplete set of nonorthogonal and nonstationary states. Removing the overcount, the remaining task is to solve the system of Eqs. (1.3.9)-(1.3.13) also known as the Bethe ansatz equations [57]. Note that we obtain particular equations for $g(1)$ and $g(2)$ corresponding to the nearest neighbor (NN) and next nearest neighbor (NNN) configurations which lead to distinct behavior and branch states in the two-magnon spectra. We explore this further in subsections 1.3.2.1 and 1.3.2.2 below. Additionally, we introduce the fidelity F as

$$F(\text{NN}, \psi) = \frac{1}{N} |\langle \text{NN} | \psi \rangle|^2 = |g(1)|^2, \quad (1.3.14)$$

where the NN state for a chain of N sites is defined as

$$|\text{NN}\rangle = \frac{1}{\sqrt{N}} \sum_{n_1=1}^N e^{iK(n_1+n_2)} |\uparrow \dots \uparrow \downarrow_{n_1} \downarrow_{n_2} \uparrow \dots \uparrow\rangle, \quad (1.3.15)$$

where $n_2 = (n_1 + 1) \bmod N$. It is defined as the probability to measure a given state $|\psi\rangle$ of momentum K and energy E in a bound state configuration corresponding to the two magnons being nearest neighbors. These bound state configurations were previously

theoretically studied in [58, 59, 60, 61, 62] and from an experimental point of view as well in [63, 64].

1.3.2.1. Ferromagnetic $J > 0$. A plot of the two-magnon energies versus wavevector K for $N = 200$ as obtained from the solutions of Eqs. (1.3.9)-(1.3.13) is shown in Fig. 1.1. The 19900 points in the range $0 \leq K \leq \pi$ produce a density plot for the two-magnon continuum which emerges in the limit $N \rightarrow \infty$ [56, 65]. The color scheme legend denoting the fidelity is also provided.

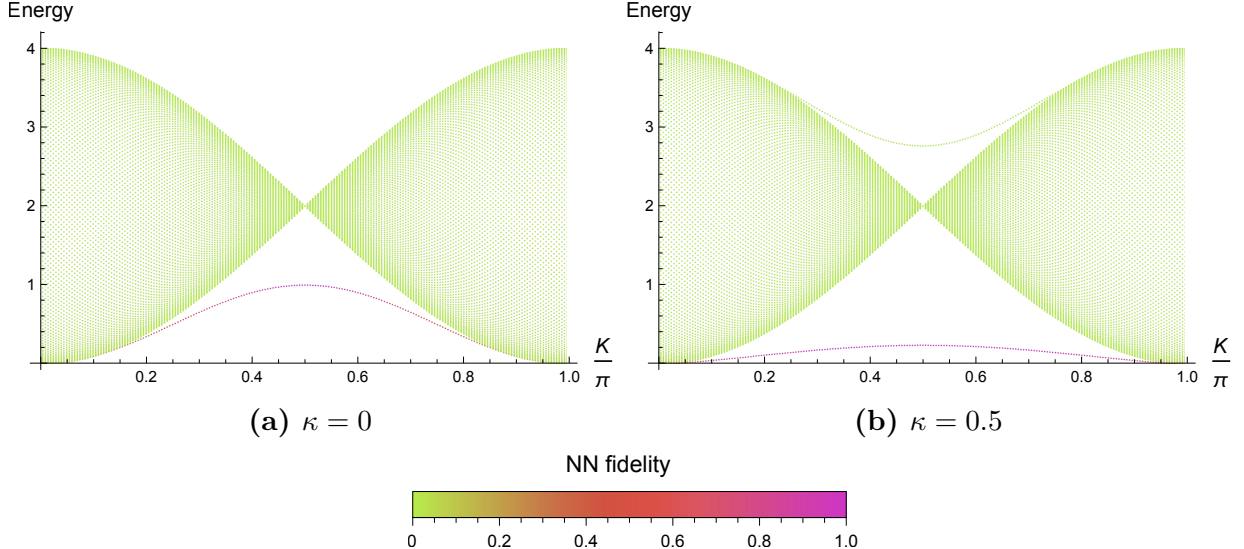


Fig. 1.1. Two-magnon excitations and nearest neighbor fidelity of the ferromagnetic quantum Ising-Kawasaki spin chain with $N = 200$ for (a) $\kappa = 0$ and (b) $\kappa = 0.5$. For $\kappa = 0$ we recover the Heisenberg XXX known result [65].

We recover in Fig. 1.1a the Heisenberg XXX continuum when taking $\kappa = 0$ in accordance with Eq. (1.2.7). Generally, two-magnons configurations correspond to 4 domain walls. However, magnons on neighboring sites correspond to 2 domain walls and require intermediate states with a larger number of domain walls implying a higher energy in order to propagate. Thus nearest neighbor configurations have a lower energy and survive as a bound state. Consequently, as can be seen for the XXX Heisenberg model, pairs of magnons form a continuum of two-magnon scattering states and a lower branch of two magnon bound states [66, 67, 58, 59]. Additionally, in Fig. 1.1b we find an upper branch of states separate from the continuum dominated by next-nearest neighbor excitations of the form $|\uparrow \dots \uparrow \downarrow \uparrow \dots \uparrow\rangle$. Consequently the lower and upper branches are respectively characterized by the Eqs. (1.3.9) and (1.3.10) for $g(1)$ and $g(2)$. The apex of each branch is found at $K = \pi/2$ as equations (1.3.9) and (1.3.10) are simplified to

$$(1 - \alpha_\kappa)g(1) = Eg(1) \quad (1.3.16)$$

$$(2 + \alpha_\kappa)g(2) = Eg(2). \quad (1.3.17)$$

The maximum of the lower branch of bound states decreases with increasing κ in the ferromagnetic case, and in the limit $\kappa \rightarrow \infty$, the bound states tend towards zero. Meanwhile, the behavior of the upper branch at large κ remains similar to what is seen in Fig. 1.1b, with its minimum increasing to $E = 3$. The two-magnon spectrum in this limit is shown in Fig. A.1a of Appendix A.1.

1.3.2.2. Antiferromagnetic $J < 0$. In the antiferromagnetic regime $\kappa < 0$, the branch states have a more intricate behavior as we now discuss. At $\kappa = 0$, we saw previously that the branch below the continuum corresponds to a bound state of the two magnons (high NN fidelity). As κ becomes negative, anti-alignement of spins is favored, implying that this branch is pushed to higher energies. In addition, a NNN branch appears, as for $\kappa > 0$. These phenomena can be seen in Fig. 1.2a-1.2b. However, in contrast to the ferromagnetic case, the NNN is now located below the continuum. As the κ becomes progressively more negative, the NNN branch shifts to lower energies, while the NN to higher energies. The inevitable collision between the two branches occurs at

$$\kappa_x = \frac{\operatorname{arctanh}(-1/2)}{2} = -\frac{\ln 3}{4} \approx -0.275, \quad (1.3.18)$$

as can be observed in Fig. 1.2c. As $\kappa \rightarrow \kappa_x$, the bound state (NN) fidelity of the NNN branch states increases. At κ_x , we find that $(1 - \alpha_\kappa) = (2 + \alpha_\kappa)$, and so the energies found in Eqs. (1.3.16) and (1.3.17) are equal and the two branches cross at $K = \pi/2$. Additionally, the fidelity of the two branches becomes the same near the crossing, as can be seen in Fig. 1.2c.

In the limit where $\kappa \rightarrow -\infty$, the bound state fidelity of the NNN branch states decreases back to 0 past κ_x . We also find that Eq. (1.3.9) becomes

$$2g(1) = Eg(1) \quad (1.3.19)$$

and the interaction term $4\gamma_\kappa(1 - \delta_\kappa)\cos(K)$ between the coupled Eqs. (1.3.9) and (1.3.10) tends to zero, meaning that we have a pure bound state not interacting with the continuum of energy $E = 2$ and fidelity 1 at every value of K . This is shown in Fig. A.1b of Appendix A.1. Consequently, the NN branch states form the upper branch of the continuum in the antiferromagnetic regime past κ_x . This limit can be observed in Fig. 1.4.

We note that throughout Fig. 1.1 to 1.2 the bowtie form of the envelope of the continuum is unchanged implying that it is independent of κ . However, the states within the envelope evolve with κ . The coupling strength of the $g(1)$ dominated states, $|4\gamma_\kappa(1 - \delta_\kappa)|$, decreases with increasing $|\kappa|$ and conversely increases as $|\kappa|$ decreases as can be seen by the black line in Fig. 1.4. For strong interactions, the quasiparticle is pushed outside of the continuum as a consequence of level repulsion [68]. This is observed in Fig. 1.2a. One would expect that as the interaction starts weakening, the bound state decays when encountering the continuum.

It is indeed the case in Fig. 1.2d. However as the coupling further decreases the bound state becomes longer lived throughout the continuum as can be seen in Fig. 1.3 and Fig. A.1b. In fact, the weaker interactions lead to a stronger NN fidelity and lower perturbation allowing for a penetration of the bound state branch through the continuum. Note that the NN fidelity observed in Fig. 1.2 is significantly lower due to a lower $|\kappa|$ leading to higher coupling in comparison with Fig. 1.3 and thus resulting in a faster decay of the branch states within the bulk of the continuum. This behaviour is particular to the antiferromagnetic regime as the bound state branch tends toward the center of the continuum at $E = 2$ with increasing fidelity in the $\kappa \rightarrow -\infty$ limit. In the ferromagnetic case, the bound state branch approaches $E = 0$ as $\kappa \rightarrow \infty$, so that the bound states remain below the continuum and no merger with the continuum occurs.

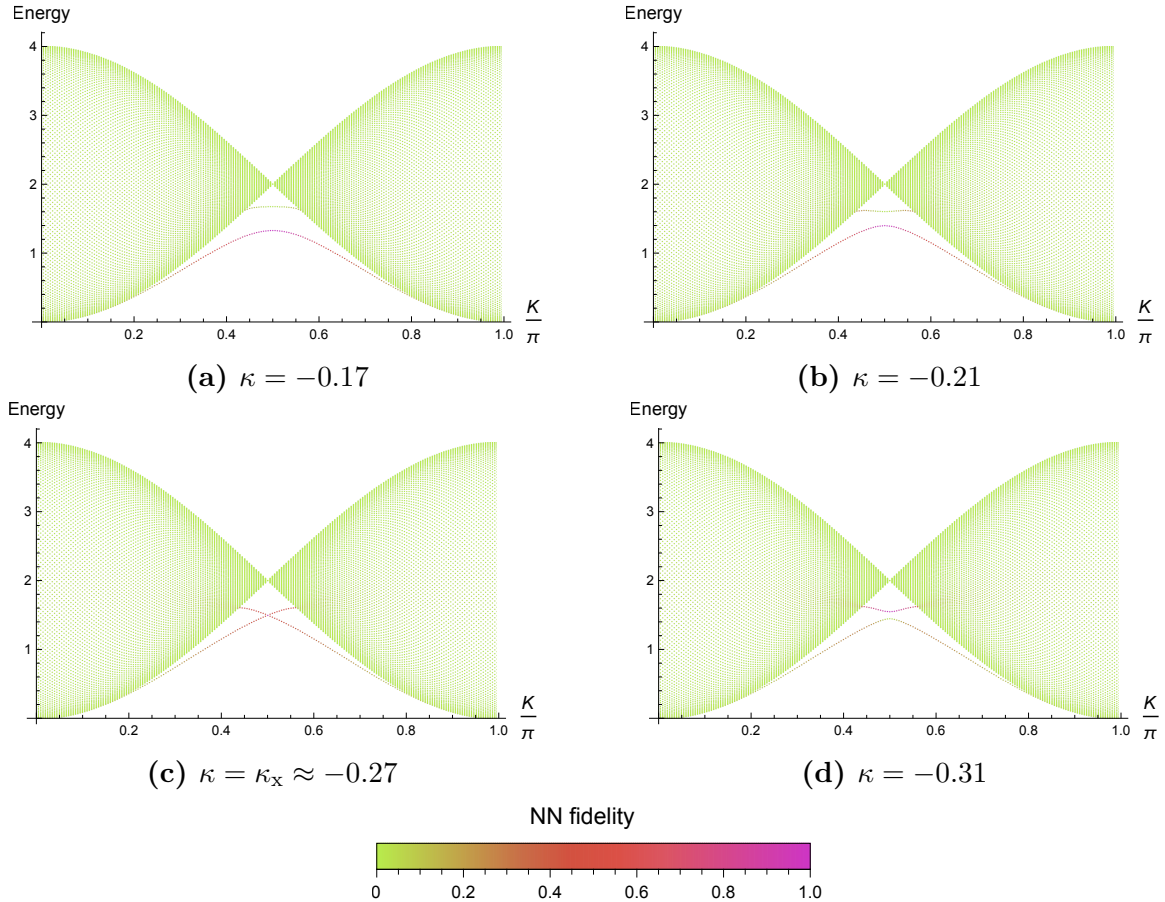


Fig. 1.2. Two-magnon excitations and nearest neighbor fidelity for the antiferromagnetic quantum Ising-Kawasaki spin chain with $N = 200$ around κ_x .

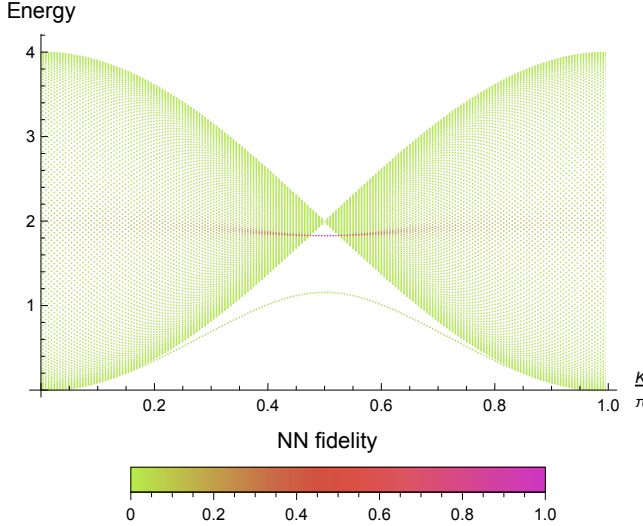


Fig. 1.3. Two-magnon excitations and nearest neighbor fidelity for $N = 200$ and $\kappa = -0.6$.

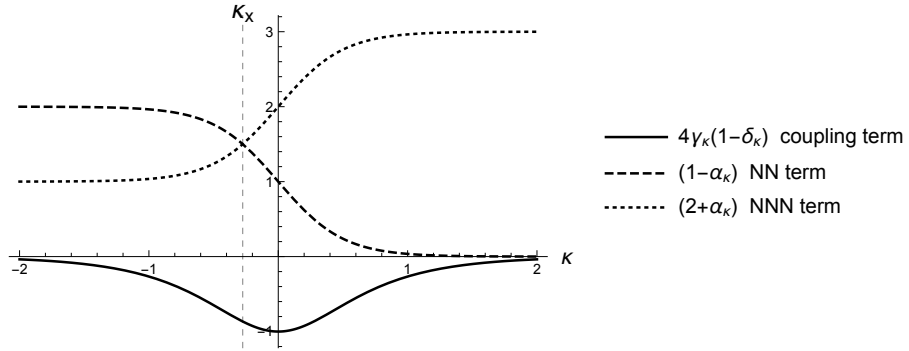


Fig. 1.4. Nearest and next-nearest neighbor branch state energies for the two-magnon excitations at $K = \pi/2$ given by Eqs. (1.3.16,1.3.17). The crossing value where the Eqs. (1.3.16,1.3.17) have the same energy at κ_x is highlighted by the grey vertical dashed line. The solid black line shows the coupling term in Eqs. (1.3.9, 1.3.10).

1.3.3. Dynamical critical exponents

The critical exponent of the 2-magnon sector can be easily deduced to be $z = 2$ from the quadratic shape of the enveloppe of the continuum, which holds for all values of the coupling κ . Note that this is the same critical exponent as obtained from Eq. (1.3.2) for the 1-magnon sector. This is also consistent with the critical exponent calculated by Grynberg for the entire spin chain with antiferromagnetic coupling $\kappa < 0$ in [9]. However, in the ferromagnetic case $\kappa > 0$, Grynberg numerically obtains a critical exponent dependent on κ , and always exceeding 2. In particular, it ranges from $z \approx 2$ at small κ , while in the limit where $\kappa \gg 1$ Grynberg finds $z \approx 3.1$ using exact diagonalization on short chains. For a range of $\kappa > 0$ values, we have found using exact diagonalization that the lowest excited states occur in the $S_z^T = 0$ sector for even chains and the $S_z^T = \pm 1/2$ sectors for odd chains,

which are substantially more complicated than the 1- or 2-magnon sectors. Furthermore, the momentum of these excited states corresponds to the smallest non-zero magnitude: $\pm 2\pi/N$. We thus see that the lowest excited level has a degeneracy of 2 for even chains, while it is 4 for odd ones. We have also found that the next excited level has the same momenta, but higher spin: $S_z^T = \pm 1$ (even chains) and $S_z^T = \pm 3/2$ (odd chains).

Grynberg's results are consistent with the known results for classical Kawasaki dynamics at large β according to which $z = 3$ is the dominant critical exponent in sectors with small $|S_T^z|$ [10, 11, 12, 13]. We recall the basic argument here. When κ is large but finite, the system rapidly reaches a metastable state via energy conserving and lowering events. Then after a long time $e^{4\kappa}$, an energy raising event overcomes the local barrier, and the system can reach a lower metastable state. Eventually, this cascade leads to the ground state. The key process is the diffusion of a spin across a domain of opposite orientation, which can be alternatively seen as the slow diffusion of the entire domain [40, 41, 42, 43]. The diffusion coefficient scales as $D(\ell) = 1/\ell$ for a domain of length ℓ , which leads to a subdiffusive domain growth $\ell \sim t^{1/3}$. This translates to a dynamical critical exponent $z = 3$ (relating energy to wavevector $E \sim k^z$). We note that in the classical statistical mechanics literature, the dynamical exponent is often defined as the inverse of the above definition: $z_c = 1/z = 1/3$. We thus see that the quantum spin chain hosts both diffusive ($z = 2$) and subdiffusive modes at $\kappa > 0$, signalling the presence of multiple dynamics at low energy. The subdiffusive modes soften as β increases, and will thus dominate certain observables. Similar phenomena were encountered in the Motzkin and Fredkin quantum spin chains (and their deformations) [47, 19]. A dynamical critical exponent of $z = 3$ was also encountered in a different $S = 1/2$ quantum spin chain studied in the context of lattice supersymmetry [69, 70]. It would be desirable to obtain a low energy description that explains the critical exponents in such systems.

1.4. Energy Level Statistics

The level spacing distribution $P(s)$ is the probability that adjacent energies have spacing s . For the following analysis, we need to work with the unfolded and unsymmetrized spectrum. The unfolded spectrum is obtained by renormalizing the energies such that the local density of states is constant and equal to one. To do so, we first compute the full spectrum in a specified symmetry sector labeled by S_T^z and k as detailed in Appendices A.2 and A.3. Then, the unfolding method presented in [35, 36] is followed to obtain the unfolded eigenvalues and their nearest neighbor level spacing s . We define the integrated density of states as $n(E) = \sum_{i=1}^D \theta(E - E_i)$, where θ is the Heaviside step function, D is the dimension of the symmetry sector and $\{E_i\}_{i=1}^D$ the energies. We then approximate its average $\langle n(E) \rangle$ via a spline interpolation through the evenly spaced sample points $(E_i, n(E_i))$ for $i \in \{1, 21, 41, \dots\}$. The size of the sample step here chosen to be 20 doesn't affect the results

when far enough from 1 and D . The unfolded eigenvalues are then defined as $x_i = \langle n(E_i) \rangle$ and their nearest neighbor spacing $s_i = x_{i+1} - x_i$ [35, 36]. According to the Berry-Tabor conjecture [30, 31], if the system is integrable, the distribution will be a negative exponential (1.4.1) describing a Poisson process:

$$P_{\text{Poi}}(s) = \exp(-s). \quad (1.4.1)$$

On the other hand, if it isn't integrable the spectrum will exhibit level repulsion and rigidity, and, for systems with time-reversal symmetry, the distribution will be the Wigner surmise (1.4.2) from the Gaussian orthogonal ensemble (GOE) of random matrix theory:

$$P_{\text{Wig}}(s) = \frac{\pi s}{2} \exp\left(-\frac{\pi s^2}{4}\right). \quad (1.4.2)$$

The distributions will be fitted with a normalized linear combination of the two distributions:

$$\alpha P_{\text{Poi}}(s) + (1 - \alpha) P_{\text{Wig}}(s). \quad (1.4.3)$$

Figure 1.5 shows the distribution for the largest symmetry sector with $S_T^z \neq 0$ and $k \notin \{0, \pi\}$ for a chain of length $N = 24$. Very strong correspondence with the Wigner distribution is observed.

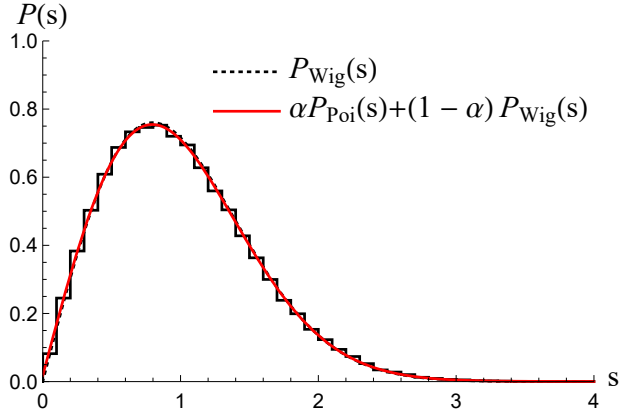


Fig. 1.5. Level spacing distribution for $N = 24$, $\kappa = 0.5$ in the $S_T^z = 1$ and $k = 2\pi/24$ symmetry sector which has 104006 states. The dashed, dotted and plain red lines represent respectively the negative exponential distribution (1.4.1), the Wigner surmise (1.4.2), and the fit (1.4.3). The fit coefficient α value obtained is 0.02.

In the $k \in \{0, \pi\}$ symmetry sectors, an extra desymmetrization step is needed to account for the spatial inversion symmetry \hat{P} . Figure 1.6 shows the distributions for both reflection eigenvalues $P = \pm 1$ in the largest symmetry sector with spatial reflection symmetry ($k = 0$) for $N = 25$. Again, Wigner distributions are observed.

Spin reversal symmetry also implies that the spectrum for S_T^z is the same as the one for $-S_T^z$. Similarly, the spatial inversion symmetry implies that the spectrum for k is the same as the one for $-k$. Figure 1.7 shows the value of the fit coefficient α in each symmetry sector

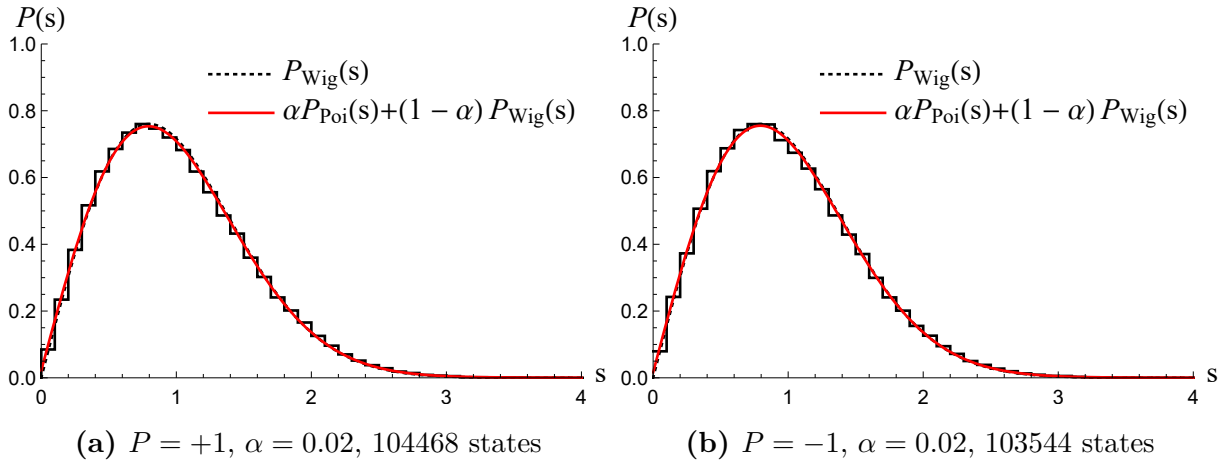


Fig. 1.6. Level spacing distribution for $N = 25$, $\kappa = 0.5$ in the $S_T^z = 1/2$, $k = 0$ and $P = \pm 1$ symmetry sector.

for $N = 20$ and $N = 21$. It is close to 0 in most cases, indicating Wigner behaviour. The same behaviour is observed for different values of κ in $[-1, -0.1]$ and $[0.1, 1]$ — the unfolding method used isn't reliable for $|\kappa| < 0.1$ and $|\kappa| > 1$ since $n(E)$ becomes highly discontinuous near 0 and the difference between consecutive energies approaches the numerical precision. Therefore, our level spacing analysis suggests that the system isn't integrable for finite, non-zero κ . The value of α increases as S_T^z increases because there are less eigenvalues so the histogram is less smooth and the quality of the fit diminishes. The same behaviour is observed for $13 \leq N \leq 19$.

Our analysis allows us to conclude that the system is not integrable for generic value of $\kappa \neq 0, \pm \infty$. This applies equally to the Hamiltonian H and the Markov operator \hat{W} , as they share the same spectrum. Our conclusion is in agreement with the known results for non-equilibrium classical Kawasaki dynamics [40].

1.5. Conclusion

To summarize, we have studied a stoquastic quantum spin-1/2 chain dual to the non-equilibrium Kawasaki dynamics of a classical Ising chain coupled to a thermal bath. After deriving the corresponding Hamiltonian for non-uniform Ising couplings, we showed that the exact groundstates are obtained from the Boltzmann distribution of the classical Ising model via a nonunitary similarity transformation given in Eq. (1.2.5). Energy level spacing distributions have revealed the model to be non-integrable for finite uniform couplings $\kappa \neq 0$. Consequently, we find that the associated non-equilibrium classical dynamics are ergodic. The one and two magnon sectors exhibit a critical exponent $z = 2$, which differs from the value $z = 3$ obtained when $\kappa \gg 1$, thus suggesting the presence of multiple dynamics at low energy. For the two-magnon sector, there is peculiar behavior in the antiferromagnetic

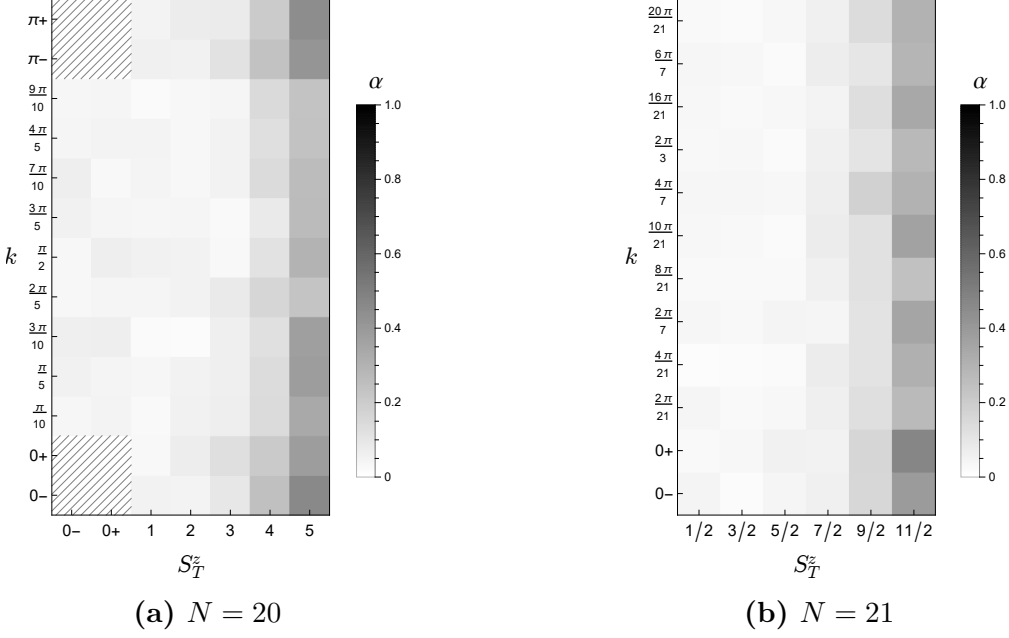


Fig. 1.7. Fit coefficient α in each symmetry sector for $N = 20$ and $N = 21$ with $\kappa = 0.5$. Values of $\alpha = 0$ and 1 correspond respectively to Wigner and Poisson distributions, respectively. The symbols $0\pm$ and $\pi\pm$ on the momentum axis k designate the symmetry sectors with $P = \pm 1$ and respectively $k = 0$ and π . Similarly, the $0\pm$ on the total z-spin axis S_T^z designate the symmetry sectors with $\mathcal{T} = \pm 1$ and $S_T^z = 0$. Here \mathcal{T} corresponds to time-reversal. Sectors with $S_T^z \geq 6$ are not shown as they are too small (< 300) to produce a good histogram.

regime past $\kappa_x = -\ln(3)/4$ as the nearest neighbor dominated branch crosses the NNN one, and starts penetrating the continuum. At $\beta = \infty$, the conservation of the Ising energy (i.e. domain wall number) leads to a multitude of frustrated states and the slowing down of the dynamics. Further work to understand the associated glassy dynamics is needed. It would also be interesting to generalize the analysis to the disordered case, as well as to higher dimensions.

From a quantum perspective, it would be interesting to examine the entanglement properties of the eigenstates. For example, one could study the quantum error correcting properties of its ground space, in the same spirit as was done for the Motzkin and other spin chains [48]. Further, given the conservation of spin, one could study the frequency-dependent spin conductivity as a function of the coupling κ , and of the temperature in the quantum system (not to be confused with the $1/\beta$ appearing in the coupling).

Acknowledgements

The authors thank X. Chen, N. Crampé, H. Katsura, M. Knap and J. Feldmeier for insightful discussions. This work was funded by a Discovery Grant from NSERC, a Canada Research Chair, a grant from the Fondation Courtois, and a “Établissement de nouveaux

chercheurs et de nouvelles chercheuses universitaires” grant from FRQNT. Simulations were performed on Calcul Québec’s and Compute Canada’s superclusters. GL is supported by a BESC M scholarship from NSERC and a B1X scholarship from FRQNT.

Article 2

Dynamics of periodic Fredkin spin chains

Par Gabriel Longpré, Stéphane Vinet et William Witczak-Krempa.

Article en préparation.

Abstract. We study the Fredkin quantum spin chain, a stoquastic or Rokshar-Kivelson like model that displays anomalous dynamics and entanglement properties. In contrast to most previous works, we use periodic boundary conditions. Through exact diagonalisation, we find that the dynamical exponent is $z = 3.23 \pm 0.20$ for even chains, while it is reduced to 2.71 ± 0.09 for odd ones. Interestingly, these exponents also appear in even chains with specific open boundary conditions, but in different symmetry sectors. The smallest exponent also matches results for Fredkin Random Unitary Circuits. We also obtain the 1- and 2-magnon spectra, that have quadratic dispersion at low energy. This establishes the presence of multiple critical dynamics. Furthermore, we find that the dispersion of certain low energy branches is anomalous: it does not converge to the naive relation Ak^z , where A is size-independent. Finally, the energy level spacing statistics are Wigner distributed, which points towards ergodic non-integrable behavior.

2.1. Introduction

Quantum many-body systems possess emergent dynamical properties that cannot be simply guessed from their time-evolution operator. For instance, the emergent Lorentz and conformal symmetries are not manifest in the 1d or 2d transverse field quantum Ising model at its transition point. Of particular interest are systems where the dynamics does not fall into known universality classes, for example a critical system not exhibiting emergent Lorentz scaling between space and time. Stoquastic Hamiltonians are a family of systems where such anomalous dynamics can be investigated in a more controlled fashion. Heuristically, a stoquastic Hamiltonian is related to a classical Markov operator. As such, it is not as “quantum” as a general Hamiltonian, but it can nevertheless possess many non-trivial properties

with the advantage of additional theoretical control. Most notably this includes generalized Rokhsar-Kivelson (RK) Hamiltonians [71]. In 1d, some quantum spin chains illustrate the rich possibilities of stoquastic/RK systems. Recently, anomalous dynamical critical exponents z that characterize the gap closing for long chains $\sim 1/N^z$ have been observed in the Motzkin, Fredkin and Kawasaki-Ising quantum spin chains [9, 44, 72, 47, 19, 73, 14]. In particular, the subdiffusive dynamical exponents for Motzkin and Fredkin chains have been numerically found to be slightly in excess of 3. Such results have been obtained with open chains under special boundary conditions.

With periodic boundary conditions, both chains possess a number of ground states that grows linearly with chain length. It would thus be important to verify whether the boundary conditions and/or parity of the chain length can alter the observed anomalous dynamics. In this work, we tackle this question for the Fredkin chain. Using exact diagonalization, we find that the periodic Fredkin chain of even length possesses the same exponent as open even chains, $z_{\text{even}} = 3.23 \pm 0.20$. For odd periodic chains, we find that the dynamical exponent is reduced to $z_{\text{odd}} = 2.71 \pm 0.09$, which matches what was found for the second excited state of even open chains [19]. We further solve for the 1- and 2-magnon excitations, and find similarities with both the XXX and Kawasaki-Ising chains, although distinct features arise. Further, our exact diagonalization suggests that the excitations in the sectors with small $|S_z|$ (large number of magnons) possess an anomalous dispersion relation not simply given by a power of the wavevector, k^z . Finally, we study the energy level spacing statistics of all states per symmetry sector, and find a Wigner distribution, indicative of a non-integrable system.

The paper is structured as follows. In Section 2.2, we present the Fredkin model, its Hamiltonian and its ground states. In Section 2.3, we find its dynamical exponents for periodic boundary conditions. In Section 2.4, we use a ansatz to obtain the one- and two-magnon excitations. In Section 2.5, we study the dispersion at low energy and find subsidence, indicating anomalous dispersion. In Section 2.6, using exact diagonalization, we obtain the level spacing distribution of the entire spectrum. Its Wigner distribution suggests that the system isn't integrable. The main results are summarised in Section 2.7.

2.2. Fredkin Spin Chain

We study the periodic Fredkin spin-1/2 chain of length N [15]. The interaction in the model comes from Fredkin gates acting on three neighboring sites: a swap of spins is performed if the control spin (in bold below) takes a given value,

$$\uparrow\uparrow\downarrow \leftrightarrow \uparrow\downarrow\uparrow \quad \uparrow\downarrow\downarrow \leftrightarrow \downarrow\uparrow\downarrow, \quad (2.2.1)$$

where in the first case the swap happens only if the control spin is up. In the second case, the swap occurs if the control spin (third one) is down. Note that the control spin is not

altered. Thus, the interaction conserves total z -spin $S_T^z = \sum_{i=1}^N \sigma_i^z / 2$. The Hamiltonian is

$$H = \sum_{i=1}^N (1 + \sigma_i^z)(1 - \vec{\sigma}_{i+1} \cdot \vec{\sigma}_{i+2}) + (1 - \vec{\sigma}_i \cdot \vec{\sigma}_{i+1})(1 - \sigma_{i+2}^z). \quad (2.2.2)$$

The first term projects the i th spin on the up state and the $(i+1)$ th and $(i+2)$ th states on the singlet state at those sites. The second term projects the $(i+2)$ th spin on the down state and the i th and $(i+1)$ th states on the singlet state at those sites. With periodic boundary conditions (PBC), translation symmetry allows further block diagonalisation using the momentum quantum number k . Unlike the Kawasaki spin chain [74], the Fredkin Hamiltonian doesn't commute with either parity P nor spin reversal R . In both cases, these operators satisfy $PHP = H' = RHR$ where

$$H' = \sum_{i=1}^N (1 - \sigma_i^z)(1 - \vec{\sigma}_{i+1} \cdot \vec{\sigma}_{i+2}) + (1 - \vec{\sigma}_i \cdot \vec{\sigma}_{i+1})(1 + \sigma_{i+2}^z). \quad (2.2.3)$$

Hence, PR is another symmetry of the system. However, it doesn't commute with total z -spin nor does it commute with the translation operator when $S_T^z \neq 0$ and $k \notin \{0, \pi\}$.

The Hamiltonian can also be expressed as the following sum of projectors:

$$H = 4 \sum_{i=1}^N \mathcal{P}(|\uparrow_i \uparrow \downarrow\rangle - |\uparrow_i \downarrow \uparrow\rangle) + \mathcal{P}(|\uparrow_i \downarrow \downarrow\rangle - |\downarrow_i \uparrow \downarrow\rangle) \quad (2.2.4)$$

where $\mathcal{P}(|\psi\rangle) = |\psi\rangle \langle \psi|$ projects onto $|\psi\rangle$. Thus, it is positive definite.

2.2.1. Ground States

The ground state energy is 0. For PBC, each $S_T^z \in \{-N/2, -N/2 + 1, \dots, N/2\}$ sector has a ground state with $k = 0$ which correspond to the ground state of the Heisenberg XXX model in that sector [15]. These states are the symmetric sum of all product states with a fixed number of up and down states. Thus, there is an equal number of terms containing $|\uparrow_i \uparrow \downarrow\rangle$ and $|\uparrow_i \downarrow \uparrow\rangle$, for all i . The symmetric sum is hence annihilated by the first projector of the Hamiltonian. Since the same argument applies for $|\uparrow_i \downarrow \downarrow\rangle$ and $|\downarrow_i \uparrow \downarrow\rangle$, it is also annihilated by the second projector. Thus, it is an eigenstate of the Hamiltonian with energy 0, i.e. a ground state, and the Hamiltonian is frustration free. When the chain length is even, the $S_T^z = 0$ sector has an extra anomalous ground state with $k = \pi$ [15]. In the $S_T^z = 0$ sector, the Fredkin relations (2.2.1) split the product state basis in two equivalence classes. The anomalous ground state is the difference between the symmetric sums of the states in each of those classes. Most of the previous work [17, 18, 19, 20, 21, 22, 23] on the Fredkin model used the boundary term $H_\partial = |\downarrow\rangle_1 \langle \downarrow| + |\uparrow\rangle_N \langle \uparrow|$ which lifts the ground states degeneracy by favoring states starting by $|\uparrow\rangle_1$ and ending by $|\downarrow\rangle_N$. With this boundary condition, the unique ground state is the symmetric combination of Dyck states [15].

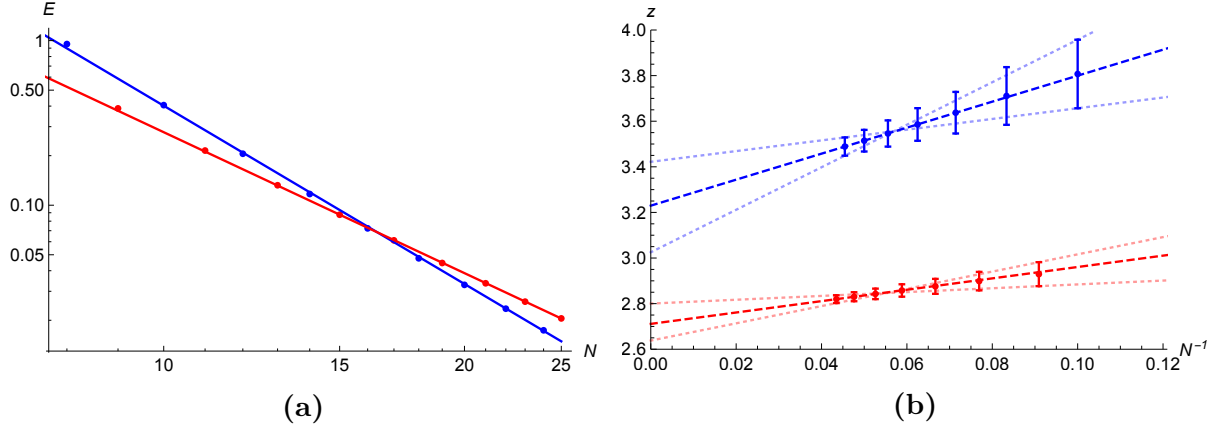


Fig. 2.1. (a) Gap scaling for even (blue) and odd (red) chain lengths fitted with $E \propto 1/N^z$. The obtained exponents are $z_{\text{even}} = 3.6$ and $z_{\text{odd}} = 2.8$. (b) Dynamical exponent linear extrapolation to $N \rightarrow \infty$ to account for finite-size effects (see appendix B.1). The blue fit is $z_{\text{even}}(N) = 3.23 + 5.70/N$ and the red one $z_{\text{odd}}(N) = 2.71 + 2.49/N$. The y -intercept corresponds to the dynamical exponent in the thermodynamical limit: $z_{\text{even}}(\infty) = 3.23 \pm 0.20$ and $z_{\text{odd}}(\infty) = 2.71 \pm 0.09$.

2.3. Dynamical exponents

Using numerical exact diagonalisation in the Bloch basis (as detailed in [74]), the whole spectrum was obtained in multiple symmetry sectors for N up to 25.

The first excitation is observed to be in the $S_T^z = \pm 1$ and $k = \pi$ sector for even N , and in the $S_T^z = \pm 1/2$ and $k = \pm(1 - 1/N)\pi$ sectors for odd N . As seen in Fig. 2.1, there is a different scaling of the energy gap for the even and odd cases. In both cases, the gap scales as $1/N^z$ for large N with the dynamical exponents $z_{\text{even}} = 3.6$ for even N and $z_{\text{odd}} = 2.8$ for odd N . A weight proportionnal to the sector's dimension of the excited state is used for the fits. However, the slope, and thus the exponent, decreases with chain length and therefore those two values are not representative of the exponent in the thermodynamical limit, especially for the even chains. To account for finite-size effects, $z(N)$ is calculated using the values for $N - 1$, N and $N + 1$. Fig. 2.1b shows that $z(N)$ scales as $1/N$. A $1/N$ extrapolation returns $z_{\text{even}}(\infty) = 3.23 \pm 0.20$ and $z_{\text{odd}}(\infty) = 2.71 \pm 0.09$. These results are within the analytical bound found by Movassagh [28]: $2 \leq z \leq 7.5$ and over the mean-field lower bound obtained by Adhikari and Beach [75]: 2.52 ± 0.01 . It is important to note that these bounds were obtained for open chains.

We believe that the difference between the dynamical exponents for odd and even lengths chains is related to the presence of an anomalous ground state in the even case. Indeed, the first excitation in the even N case is in the same momentum $k = \pi$ sector as the anomalous ground state. However, for the odd N case, there is no such ground state and the first excitation correspond to the lowest energy state of its momentum sector.

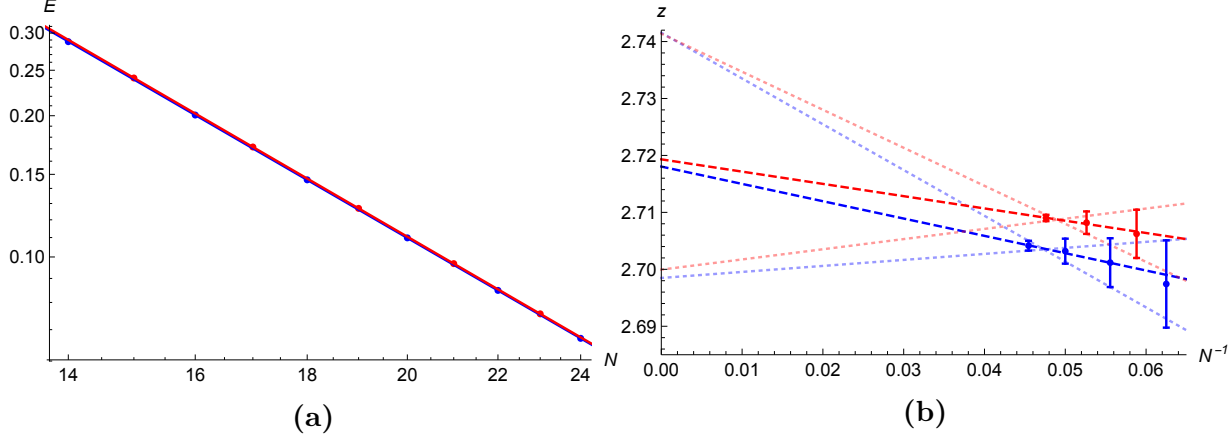


Fig. 2.2. (a) Gap scaling in the $k_1 = 2\pi/N$ momentum sector for even (blue) and odd (red) chain lengths fitted with $E = a/N^z$. The obtained exponents are $z_{k_1,\text{even}} = 2.7$ and $z_{k_1,\text{odd}} = 2.7$. (b) Dynamical exponent linear extrapolation to $N \rightarrow \infty$ to account for finite size effect (see appendix B.1). The blue fit is $z_{k_1,\text{even}}(N) = 2.72 - 0.304/N$ and the red one $z_{k_1,\text{odd}}(N) = 2.72 - 0.216/N$. The y -intercept correspond to the dynamical exponent in the thermodynamical limit: $z_{k_1,\text{even}}(\infty) = 2.72 \pm 0.02$ and $z_{k_1,\text{odd}}(\infty) = 2.72 \pm 0.02$.

At low k , the excited states with the lowest energy are in the $S_T^z = 0$ (even N) and $1/2$ (odd N) sectors. The former is also the lowest excited state of the $S_T^z = 0$ sector and the latter the second excitation of the $S_T^z = \pm 1/2$ sectors. Again, the energy of that excitation scales as $1/N^z$ for large N with the dynamical exponents $z_{k_1,\text{even}} = z_{k_1,\text{odd}} = 2.7$ for even and odd N . With the same procedure to account for finite size effects, we obtain $z_{k_1,\text{even}}(\infty) = z_{k_1,\text{odd}}(\infty) = 2.72 \pm 0.02$ which is close to $z_{\text{odd}}(\infty) = 2.71 \pm 0.09$. It is also consistent with the $S_T^z = 0$ dynamical exponents $z_0 = 2.69$ obtained by Chen *et al.* [19] (and near the 2.9 obtained by Dell'Anna *et al.* [17]), obtained with fixed boundary conditions.

2.4. Spin wave solutions

The translationally invariant basis completely diagonalizes the one-magnon sector (the $S_T^z = N/2 - 1$ block of H). Consequently, similarly to the Heisenberg XXX spin chain, the eigenvectors of H are given by the translationally invariant basis vectors:

$$|\psi\rangle = \frac{1}{\sqrt{N}} \sum_{n=1}^N e^{ikn} |n\rangle, \quad \text{where} \quad |n\rangle = |\uparrow \dots \uparrow \downarrow_n \uparrow \dots \uparrow\rangle \quad (2.4.1)$$

with wave number $k = 2\pi m/N$ and $m = 0, 1, \dots, N-1$. The eigenvalues of these translationally invariant basis vectors are given by

$$E_m = 1 - \cos(2\pi m/N), \quad (2.4.2)$$

and thus the dynamical critical exponent for the one-magnon sector is $z = 2$.

In the two-magnon sector ($S_T^z = N/2 - 2$), we use the following ansatz in the center of mass $K = k_1 + k_2$, with relative coordinate $j = n_2 - n_1$:

$$|\psi\rangle = \sum_{1 \leq n_1 < n_2 \leq N}^N a(n_1, n_2) |n_1, n_2\rangle \quad \text{where} \quad a(n_1, n_2) = e^{iK(n_1+n_2)} g(j) \quad (2.4.3)$$

and $|n_1, n_2\rangle = |\uparrow \dots \uparrow \downarrow_{n_1} \uparrow \dots \uparrow \downarrow_{n_2} \uparrow \dots \uparrow\rangle$.

The momentum of the center of mass is $K = m\pi/N$ with $m = 0, 1, \dots, N-1$. By acting on the ansatz states with the Hamiltonian and imposing an eigenstate equation, we obtain linear equations for $g(j)$. These equations depend of the parity of N and m :

$$Eg(1) = 8g(1) - 8 \exp(-iK) g(2), \quad (2.4.4)$$

$$Eg(2) = -8 \exp(iK) g(1) + 16g(2) + 8 \cos(K) g(3), \quad (2.4.5)$$

$$Eg(j) = -8 \cos(K) g(j-1) + 16g(j) - 8 \cos(K) g(j+1) \quad \text{for } 3 \leq j < (N-1)/2, \quad (2.4.6)$$

$$\begin{aligned} Eg\left(\frac{N - (N \bmod 2)}{2}\right) \\ = \begin{cases} -16 \cos(K) g(N/2 - 1) + 16g(N/2) & \text{for even } N \text{ and even } m \\ 16g(N/2) & \text{for even } N \text{ and odd } m \\ -8 \cos(K) g(\frac{N-3}{2}) + (16 - 8 \cos(K)) g(\frac{N-1}{2}) & \text{for odd } N \text{ and even } m \\ -8 \cos(K) g(\frac{N-3}{2}) + (16 + 8 \cos(K)) g(\frac{N-1}{2}) & \text{for odd } N \text{ and odd } m \end{cases}, \end{aligned} \quad (2.4.7)$$

$$g(j) = \exp(im\pi) g(N-j) \quad \text{if } N/2 < j < N. \quad (2.4.8)$$

For even N and odd m , Eq. (10) is trivially satisfied by $E = 16$. This result would however yield an overcomplete set of nonorthogonal and nonstationary states. This energy and its corresponding eigenstate are thus removed from the spectrum.

We obtain particular equations for the nearest neighbor (NN) and next nearest neighbor (NNN) configurations corresponding to Eqs. 2.4.4-2.4.5. This leads to distinct behavior and branch states for $g(1)$ and $g(2)$ in the two-magnon spectra.

Consider the following NN fidelity measurement $F(\text{NN}, \psi)$ which we define as

$$F(\text{NN}, \psi) = \frac{1}{N} |\langle \text{NN} | \psi \rangle|^2 = |g(1)|^2, \quad (2.4.9)$$

where the NN state for a chain of N sites is defined as

$$|\text{NN}\rangle = \frac{1}{\sqrt{N}} \sum_{n_1=1}^N e^{iK(n_1+n_2)} |\uparrow \dots \uparrow \downarrow_{n_1} \downarrow_{n_2} \uparrow \dots \uparrow\rangle, \quad (2.4.10)$$

where $n_2 = (n_1 + 1) \bmod N$. The fidelity is defined as the probability to measure a given state $|\psi\rangle$ of momentum K and energy E in a bound state configuration corresponding to

the two magnons being nearest neighbors. These bound state configurations were previously theoretically studied in [58, 59, 60, 61, 62, 56] and from an experimental point of view as well in [63, 64]. In the same fashion, we can define the NNN fidelity measurement $F(\text{NNN},\psi)$ with the state $|\text{NNN}\rangle$ where the magnons are separated by one site and where $n_2 = (n_1 + 2) \bmod N$.

From the solutions of Eqs. (2.4.4)-(2.4.8), we can plot the two-magnon spectrum as a function of the momentum K . For $N = 200$, the 19900 points in the range $0 \leq K < \pi$ produce a density plot for the two-magnon continuum which emerges in the limit $N \rightarrow \infty$ and is shown in Fig. 2.3. The fidelity measurement is characterized by the color scheme legend provided in Fig. 2.3.

The lower branch is dominated by nearest neighbor interactions ($F(\text{NN},\psi_1) \approx 0.7$ and $F(\text{NNN},\psi_1) \approx 0.3$). On the other hand, the upper branch is dominated by next nearest neighbor interactions ($F(\text{NN},\psi_1) \approx 0.3$ and $F(\text{NNN},\psi_1) \approx 0.7$). The scattering states continuum is the same as for Heisenberg XXX [65] and Kawasaki spin chains [74].

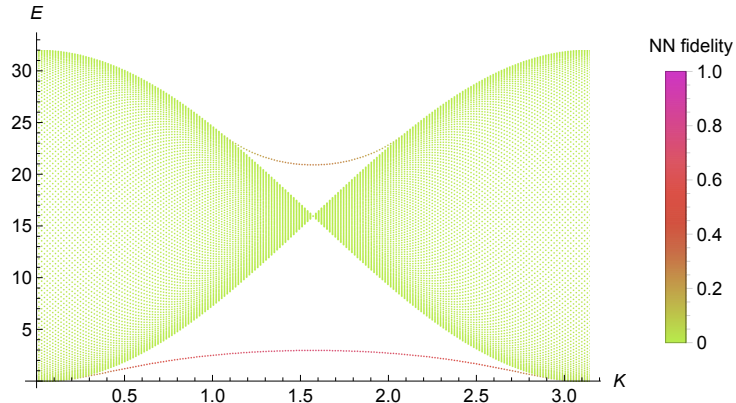


Fig. 2.3. Two-magnon excitations and nearest neighbor fidelity of the periodic Fredkin spin chain with $N = 200$.

2.5. Dispersion

Unlike in the two-magnon sector, it appears that the dispersion in lower S_T^z sectors depends on the chain length N which indicates anomalous behavior. For low momentum k , the first excitation is in the $S_T^z = 0$ (even N) and $1/2$ (odd N) sectors. The lowest energies of those sectors with respect to the momentum k is shown in Fig. 2.4. It shows that the bands subside as N increases. We also observe that they can be approximated by fits of the form $a k^b (\pi - k)^b$. However, our chains are too short to conclude on the behaviour of a_N and b_N at large N since the lowest momentum $2\pi/N$ is still large for $N = 14$ to 23 .

We can verify if the obtained values are coherent with the results from section 2.3. The energy scaling of the excitation of lowest momentum depends on the scaling of a_N and the

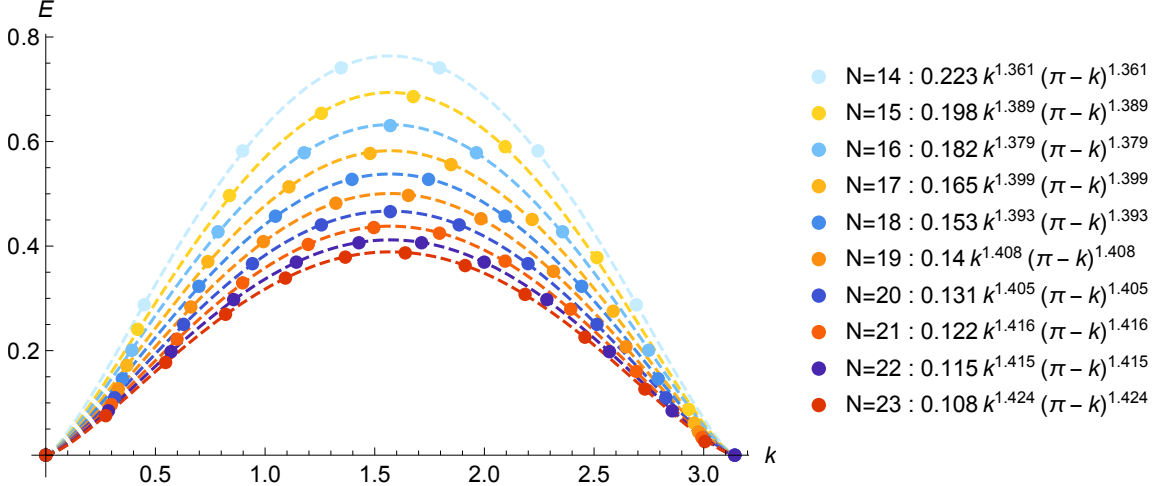


Fig. 2.4. Dispersion relation for the first excitations of the $S_T^z = 0$ (even N) and $1/2$ (odd N) sectors which host the lowest energies of the spectrum at low k . Dashed lines represent fits of the form $a k^b (\pi - k)^b$.

value of b_N at large N . As discussed in appendix B.2, the fit coefficient a_N seems to scale as $1/N^{z_a}$ with $z_a \approx 1.4$. However, using a similar procedure as in 2.3 to account for finite size effects, results suggest that z_a might be smaller (≈ 1.1 to 1.2) for large N . At $N = 23$, b_N is still increasing with a slowly decreasing slope. (Assuming that b_N scales as $1/N$ leads to $b_\infty \approx 1.5$). Using $b_N \approx b_{23} = 1.4$, at low k ,

$$E \approx a_N k^{b_N} \approx \left(\frac{9.6}{N^{1.4}} \right) \left(\frac{2\pi}{N} \right)^{b_N} \propto \left(\frac{1}{N} \right)^{1.4+b_N} \approx \left(\frac{1}{N} \right)^{1.4+1.4} = \left(\frac{1}{N} \right)^{2.8} \quad (2.5.1)$$

where 2.8 is close to the dynamical exponents $z_{k_1, \text{even}}(\infty) = 2.72$ and $z_{k_1, \text{odd}}(\infty) = 2.72$ obtained for this excitation.

In [14], Singh *et al.* numerically determine the dynamical exponent for a number of constrained charge conserving Random Unitary Circuits. They find universality classes with diffusive, subdiffusive, quasilocalized, and localized dynamics, depending on the type of constraints. In particular, they show that quantum systems with "Fredkin" constraints exhibit anomalous transport with dynamical exponent $z \approx 8/3 \approx 2.67$.

The critical exponent being different in the weakly polarized sectors ($z = 2.7$) than in the one- and two-magnon sectors ($z = 2$), the Fredkin spin chain hosts both subdiffusive and diffusive modes. This indicates the presence of multiple dynamics at low energy. For the even N case, there is also a third value of z near 3.2 at momentum π .

2.6. Energy Level Statistics

For the following analysis, we work with the unfolded and unsymmetrized spectrum. This allows the study of universal statistical properties of the Hamiltonian [76]. Using the Bloch basis, we block diagonalize the Hamiltonian with respect to its symmetry sectors labeled by

S_T^z and k as detailed in appendices B and C of [74]. Thus, we obtain the full spectrum in each sector. We unfold those spectrums by renormalizing the energies such that the local density of states is constant and equal to one. To achieve this, the unfolding method presented in [35, 36] is used to compute the level spacing distribution $P(s)$, i.e. the probability that adjacent unfolded energies have a spacing s .

The Berry-Tabor conjecture [30, 31] states that, if the system is integrable, the level spacing distribution $P(s)$ should be a negative exponential describing a Poisson process:

$$P_{\text{Poi}}(s) = \exp(-s). \quad (2.6.1)$$

In the context of quantum spin chains, the integrability of the system corresponds to a complete solvability by the coordinate Bethe ansatz. Conversely, if the system is not integrable, for systems with time-reversal symmetry, the level spacing distribution should be the Wigner surmise from the Gaussian orthogonal ensemble (GOE) of random matrix theory:

$$P_{\text{Wig}}(s) = \frac{\pi s}{2} \exp\left(-\frac{\pi s^2}{4}\right). \quad (2.6.2)$$

As this distribution goes to 0 at $s = 0$, it characterizes spectrums that exhibit level repulsion and rigidity. To compare the distributions of the Fredkin spin chain spectrums with $P_{\text{Poi}}(s)$ and $P_{\text{Wig}}(s)$, they are fitted with a normalized linear combination of the two distributions:

$$\alpha P_{\text{Poi}}(s) + (1 - \alpha) P_{\text{Wig}}(s). \quad (2.6.3)$$

The distribution for one of the largest symmetry sectors of a chain of length $N = 25$ is shown in Fig. 2.5. We observe a strong correspondence with the Wigner distribution. Figure 2.6 shows the value of the fit coefficient α in different symmetry sectors of the Fredkin spin chain with $N = 20$ and $N = 21$. Again, we observe a strong correspondence with the Wigner distribution as the fit coefficient is close to 0 in most cases. Therefore, our level spacing analysis suggests that the system isn't integrable. As S_T^z increases, the value of α increases because there are less eigenvalues. With a smaller sample, the histogram is less smooth and the quality of the fit diminishes. The same behaviour is observed for $13 \leq N \leq 19$.

2.7. Conclusion

To summarize, we have studied a frustration free critical quantum spin-1/2 chain, the Fredkin spin chain, with periodic boundary conditions. Spin wave solutions are obtained in the one- and two-magnon sectors. The two-magnon spectrum has the same scattering state continuum as the Heisenberg XXX [65] and Kawasaki spin chains [74]. Those two sectors have a critical exponent $z = 2$. However, in the weakly polarized sectors sectors, where the first excitations are, different values were found. The first excitation has a critical exponent $z = 3.23$ for even N and 2.71 for odd N . At low momentum, the critical exponent

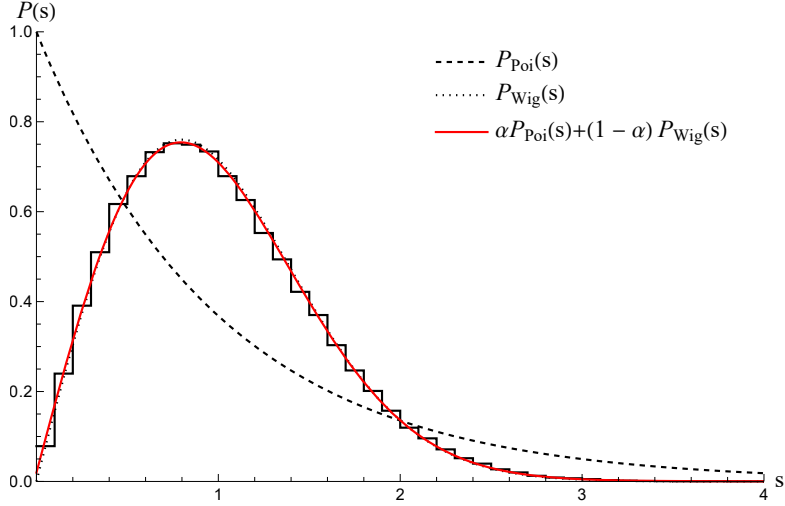


Fig. 2.5. Level spacing distribution for $N = 25$ in the $S_T^z = 1/2$ and $k = 24\pi/25$ symmetry sector which has 208012 states. The dashed, dotted and plain red lines represent respectively the negative exponential distribution (2.6.1), the Wigner surmise (2.6.2), and the fit (2.6.3). The fit coefficient α value obtained is 0.020.

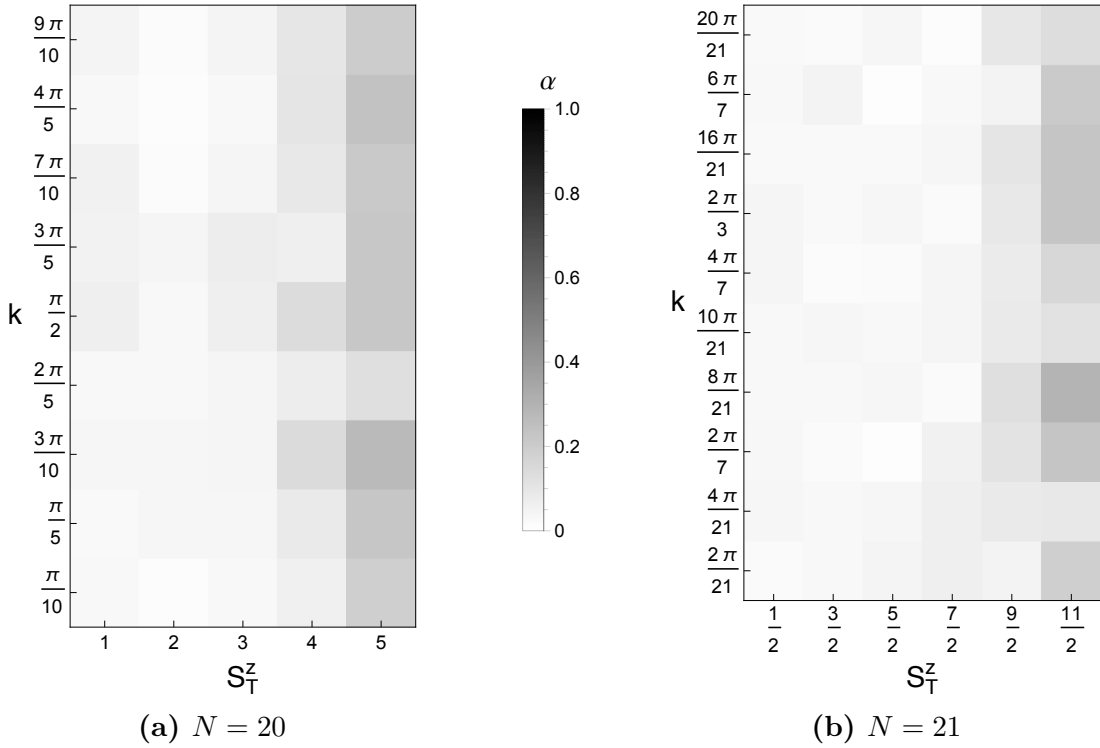


Fig. 2.6. Fit coefficient α in different symmetry sectors for $N = 20$ and $N = 21$. Values of $\alpha = 0$ and 1 correspond respectively to Wigner and Poisson distributions. Sectors with $S_T^z = 0$, $k = 0$ and $k = \pi$ are not shown since they need further desymmetrization. Sectors with $S_T^z \geq 6$ are not shown as they are too small (< 300) to produce a smooth histogram.

is $z = 2.72$ for both parity. The results for even N are consistent with exponents obtained for fixed boundary conditions [28, 17, 19, 75]. The presence of different critical exponent values suggests the existence of multiple dynamics at low energy. Unlike in the two-magnon sector, the dispersion band at low energy exhibit subsidence as N increases, which indicates anomalous behavior. Energy level statistics have revealed that the chain is non-integrable. Hence, the non-equilibrium classical dynamics associated to the quantum spin chain [28, 19] are ergodic.

A natural extension would be to study the fate of the dynamics when a positive coefficient different from one is included in Eq. 2.2.2. This preserves the ground states for the Fredkin model, but alters the dynamics. It would also be interesting to study the periodic Motzkin model, in order to see if similar parity effects are observed.

Acknowledgements

The authors thank J. Feldmeier, M. Knap and R. Vasseur for insightful discussions. This work was funded by a Discovery Grant from NSERC, a Canada Research Chair, a grant from the Fondation Courtois, and a “Établissement de nouveaux chercheurs et de nouvelles chercheuses universitaires” grant from FRQNT. Simulations were performed on Calcul Québec’s and Compute Canada’s superclusters. GL is supported by a BESC M scholarship from NSERC and a B1X scholarship from FRQNT.

Conclusion

Dans ce mémoire, nous avons étudié deux chaînes de spins quantiques critiques avec conditions frontière périodiques, soit les chaînes d’Ising–Kawasaki et de Fredkin. Nous y avons étudié l’intégrabilité, la dispersion et la dynamique. En premier lieu, la statistique des niveaux d’énergie révèle une rigidité spectrale et une répulsion des niveaux caractérisée par la distribution de Wigner. Cela indique que la chaîne de Fredkin et celle d’Ising–Kawasaki, avec κ fini et non nul, sont non intégrables. En second lieu, les secteurs à un et deux magnons ont des solutions sous forme d’ondes de spin pour les deux chaînes. L’étude de la dispersion dans le secteur à deux magnons permet d’identifier le même continuum de diffusion que celui de la chaîne XXX d’Heisenberg. Pour les deux secteurs de forte polarisation, cette dispersion révèle un exposant dynamique $z = 2$. Les deux chaînes présentent également deux branches détachées contrairement à la chaîne XXX qui n’en contient qu’une. Ces branches correspondent à des états liés. En troisième lieu, à basse énergie dans les secteurs faiblement polarisés de la chaîne de Fredkin, la bande d’états liés s’affaisse lorsque la chaîne s’allonge, ce qui indique une dispersion anomale. En combinant cet affaissement avec l’exposant dynamique à impulsions fixées, l’exposant dynamique critique obtenu est $z = 2.8$. En quatrième lieu, une étude de la croissance d’échelle de l’écart d’énergie permet d’obtenir l’exposant dynamique critique de la chaîne de Fredkin dans divers secteurs de polarisation et d’impulsion. Contrairement à la chaîne d’Ising–Kawasaki et d’Heisenberg, la première excitation de la chaîne de Fredkin a une impulsions près de $k = \pi$. La variation d’échelle de l’écart d’énergie de cette excitation correspond à un exposant critique $z = 3.23 \pm 0.20$ pour les chaînes de longueur paire et $z = 2.71 \pm 0.09$ pour les chaînes de longueur impaire. La dépendance de l’exposant sur la parité est liée à la présence d’un état fondamental anomal dans ce secteur d’impulsion $k = \pi$ pour les chaînes de longueur paire uniquement. Pour la première excitation à basse impulsions, l’exposant dynamique est plutôt $z = 2.72 \pm 0.02$ pour les chaînes de Fredkin de longueur paire et impaire. Ainsi, la cooccurrence de différents exposants critiques indique la présence de multiples dynamiques à basse énergie. En effet, même pour la chaîne d’Ising–Kawasaki, l’exposant est plutôt $z = 3$ dans le spectre complet à fort couplage.

Le modèle d’Ising avec une dynamique de Kawasaki est utilisé pour décrire les transitions de phase dans un alliage binaire. Ces matériaux présentent typiquement une interaction bi ou tridimensionnelle. Ainsi, il serait intéressant de considérer la dynamique des deux systèmes généralisés à deux et trois dimensions. Nous pourrions également vérifier s’il est possible d’obtenir des solutions d’ondes de spin dans le secteur à trois magnons en y étudiant la statistique des niveaux d’énergie. Aussi, les techniques présentées dans ce mémoire pourraient être utilisées sur la chaîne de Fredkin déformée et colorée [18, 20, 21, 77, 78]. Également, d’un point de vue quantique, il serait intéressant d’examiner le comportement de l’intrication des états propres de la chaîne d’Ising–Kawasaki et de comparer les résultats obtenus à ceux de la littérature pour la chaîne de Fredkin. Cela permettrait de mieux comprendre l’origine de la transgression de la loi du périmètre. Finalement, les résultats obtenus soulèvent une question importante sur l’origine des multiples dynamiques observées. Trouver une théorie des champs qui encapsule ces dynamiques permettrait d’expliquer leur provenance et de mieux comprendre leur dépendance sur les paramètres physiques.

Références bibliographiques

- [1] John B. PARKINSON et Damian J. J. FARRELL : *An Introduction to Quantum Spin Systems*. Springer, août 2010.
- [2] I. PESCHEL et V. J. EMERY : Calculation of spin correlations in two-dimensional ising systems from one-dimensional kinetic models. *Zeitschrift für Physik B Condensed Matter*, 43(3):241–249, 1981.
- [3] Paul RUJÁN : Exact disorder solutions. In N. SANCHEZ, éditeur : *Non-Linear Equations in Classical and Quantum Field Theory*, Lecture Notes in Physics, pages 286–300, Berlin, Heidelberg, 1985. Springer.
- [4] G. M. SCHÜTZ : 1 - Exactly Solvable Models for Many-Body Systems Far from Equilibrium. In C. DOMB et J. L. LEBOWITZ, éditeurs : *Phase Transitions and Critical Phenomena*, volume 19, pages 1–251. Academic Press, 2001. ISSN: 1062-7901.
- [5] S SANDOW et S TRIMPER : Aggregation processes in a master-equation approach. *Europhysics Letters (EPL)*, 21(8):799–804, mar 1993.
- [6] Mehran KARDAR, Giorgio PARISI et Yi-Cheng ZHANG : Dynamic scaling of growing interfaces. *Phys. Rev. Lett.*, 56:889–892, Mar 1986.
- [7] Maxime DUPONT et Joel E. MOORE : Universal spin dynamics in infinite-temperature one-dimensional quantum magnets. *Phys. Rev. B*, 101:121106, Mar 2020.
- [8] Kyozi KAWASAKI : Diffusion constants near the critical point for time-dependent ising models. i. *Physical Review*, 145(1):224–230, May 1966.
- [9] Marcelo D. GRYNBERG : Revisiting kawasaki dynamics in one dimension. *Physical Review E*, 82(5):051121, Nov 2010.
- [10] Ya'akov ACHIAM : Diffusion in the one-dimensional ising model. *Journal of Physics A: Mathematical and General*, 13(5):1825–1833, may 1980.
- [11] David A. HUSE : Corrections to late-stage behavior in spinodal decomposition: Lifshitz-slyozov scaling and monte carlo simulations. *Phys. Rev. B*, 34:7845–7850, Dec 1986.
- [12] B. D. GAULIN : Kinetics of spinodal decomposition in one dimension. *Phys. Rev. B*, 38:7184–7187, Oct 1988.
- [13] A. J. BRAY : Exact renormalization-group results for domain-growth scaling in spinodal decomposition. *Phys. Rev. Lett.*, 63:818–818, Aug 1989.
- [14] Hansveer SINGH, Brayden A WARE, Romain VASSEUR et Aaron J FRIEDMAN : Subdiffusion and many-body quantum chaos with kinetic constraints. *Physical Review Letters*, 127(23):230602, 2021.
- [15] Olof SALBERGER et Vladimir KOREPIN : Fredkin Spin Chain. In *Ludwig Faddeev Memorial Volume*, pages 439–458. WORLD SCIENTIFIC, octobre 2017.
- [16] Sergey BRAVYI, Libor CAHA, Ramis MOVASSAGH, Daniel NAGAJ et Peter SHOR : Criticality without frustration for quantum spin-1 chains. *Physical Review Letters*, 109(20):207202, novembre 2012. arXiv: 1203.5801.

- [17] L. DELL'ANNA, O. SALBERGER, L. BARBIERO, A. TROMBETTONI et V. E. KOREPIN : Violation of cluster decomposition and absence of light cones in local integer and half-integer spin chains. *Physical Review B*, 94(15):155140, octobre 2016. Publisher: American Physical Society.
- [18] Olof SALBERGER, Takuma UDAGAWA, Zhao ZHANG, Hosho KATSURA, Israel KLICH et Vladimir KOREPIN : Deformed Fredkin spin chain with extensive entanglement. *Journal of Statistical Mechanics: Theory and Experiment*, 2017(6):063103, juin 2017. Publisher: IOP Publishing.
- [19] Xiao CHEN, Eduardo FRADKIN et William WITCZAK-KREMPA : Gapless quantum spin chains: multiple dynamics and conformal wavefunctions. *Journal of Physics A: Mathematical and Theoretical*, 50(46):464002, octobre 2017. Publisher: IOP Publishing.
- [20] Zhao ZHANG et Israel KLICH : Entropy, gap and a multi-parameter deformation of the Fredkin spin chain. *Journal of Physics A: Mathematical and Theoretical*, 50(42):425201, septembre 2017. Publisher: IOP Publishing.
- [21] Takuma UDAGAWA et Hosho KATSURA : Finite-size gap, magnetization, and entanglement of deformed Fredkin spin chain. *Journal of Physics A: Mathematical and Theoretical*, 50:405002, septembre 2017. Publisher: IOP Publishing.
- [22] Luca DELL'ANNA : Long-distance entanglement in Motzkin and Fredkin spin chains. *SciPost Physics*, 7(4):053, octobre 2019.
- [23] L. DELL'ANNA, L. BARBIERO et A. TROMBETTONI : Dynamics and correlations in Motzkin and Fredkin spin chains. *Journal of Statistical Mechanics: Theory and Experiment*, 2019(12):124025, décembre 2019. Publisher: IOP Publishing.
- [24] Ramis MOVASSAGH et Peter W. SHOR : Power law violation of the area law in quantum spin chains. *Proceedings of the National Academy of Sciences*, 113(47):13278–13282, novembre 2016. arXiv: 1408.1657.
- [25] Fumihiko SUGINO et Vladimir KOREPIN : Rényi entropy of highly entangled spin chains. *International Journal of Modern Physics B*, 32(28):1850306, novembre 2018. Publisher: World Scientific Publishing Co.
- [26] Fumihiko SUGINO : Highly Entangled Spin Chains and 2D Quantum Gravity. *Symmetry*, 12(6):916, juin 2020. Number: 6 Publisher: Multidisciplinary Digital Publishing Institute.
- [27] Vladimir E KOREPIN : Universality of entropy scaling in one dimensional gapless models. *Physical review letters*, 92(9):096402, 2004.
- [28] Ramis MOVASSAGH : The gap of Fredkin quantum spin chain is polynomially small. *Annals of Mathematical Sciences and Applications*, 3(2):531–562, 2016. arXiv: 1609.09160.
- [29] IC PERCIVAL : Regular and irregular spectra. *Journal of Physics B: Atomic and Molecular Physics*, 6(9):L229, 1973.
- [30] Michael Victor BERRY et Michael TABOR : Level clustering in the regular spectrum. *Proceedings of the Royal Society of London. A*, 356(1686):375–394, September 1977.
- [31] O. BOHIGAS, M. J. GIANNONI et C. SCHMIT : Characterization of Chaotic Quantum Spectra and Universality of Level Fluctuation Laws. *Physical Review Letters*, 52(1):1–4, janvier 1984.
- [32] Henrik BRUUS et Jean-Christian ANGLES D'AURIAC : Energy level statistics of the two-dimensional hubbard model at low filling. *Physical Review B*, 55(14):9142, 1997.
- [33] Barnali CHAKRABARTI, Anindya BISWAS, VKB KOTA, Kamalika ROY et Sudip Kumar HALDAR : Energy-level statistics of interacting trapped bosons. *Physical Review A*, 86(1):013637, 2012.
- [34] Fritz HAAKE : Quantum signatures of chaos. In *Quantum Coherence in Mesoscopic Systems*, pages 583–595. Springer, 1991.

- [35] Kazue KUDO et Tetsuo DEGUCHI : Unexpected non-wigner behavior in level-spacing distributions of next-nearest-neighbor coupled XXZ spin chains. *Physical Review B*, 68(5):052510, Aug 2003.
- [36] Kazue KUDO et Tetsuo DEGUCHI : Level statistics of XXZ spin chains with a random magnetic field. *Physical Review B*, 69(13):132404, Apr 2004.
- [37] P. RUJÁN : Order and disorder lines in systems with competing interactions: I. Quantum spins at $T=0$. *Journal of Statistical Physics*, 29(2):231–245, octobre 1982.
- [38] C L HENLEY : From classical to quantum dynamics at rokhsar-kivelson points. *Journal of Physics: Condensed Matter*, 16(11):S891–S898, mar 2004.
- [39] S. V. ISAKOV, P. FENDLEY, A. W. W. LUDWIG, S. TREBST et M. TROYER : Dynamics at and near conformal quantum critical points. *Physical Review B*, 83(12), Mar 2011.
- [40] Pavel L. KRAPIVSKY, Sidney REDNER et Eli BEN-NAIM : *A Kinetic View of Statistical Physics*. Cambridge University Press, 2010.
- [41] Stephen J. CORNELL, Kimmo KASKI et Robin B. STINCHCOMBE : Domain scaling and glassy dynamics in a one-dimensional kawasaki ising model. *Phys. Rev. B*, 44:12263–12274, Dec 1991.
- [42] E. BEN-NAIM et P. L. KRAPIVSKY : Domain number distribution in the nonequilibrium ising model. *Journal of Statistical Physics*, 93(3):583–601, 1998.
- [43] Claude GODRÈCHE, Florent Krzaka A et Federico RICCI-TERSENGHI : Non-equilibrium critical dynamics of the ferromagnetic ising model with kawasaki dynamics. *Journal of Statistical Mechanics: Theory and Experiment*, 2004(04):P04007, may 2004.
- [44] Sergey BRAVYI, Libor CAHA, Ramis MOVASSAGH, Daniel NAGAJ et Peter W. SHOR : Criticality without frustration for quantum spin-1 chains. *Phys. Rev. Lett.*, 109:207202, Nov 2012.
- [45] Ramis MOVASSAGH et Peter W. SHOR : Supercritical entanglement in local systems: Counterexample to the area law for quantum matter. *Proceedings of the National Academy of Sciences*, 113(47):13278–13282, 2016.
- [46] Olof SALBERGER et Vladimir KOREPIN : *Fredkin Spin Chain*, pages 439–458. World Scientific, 2018.
- [47] Xiao CHEN, Eduardo FRADKIN et William WITCZAK-KREMPA : Quantum spin chains with multiple dynamics. *Physical Review B*, 96(18), Nov 2017.
- [48] Fernando G. S. L. BRANDÃO, Elizabeth CROSSON, M. Burak ŞAHINOĞLU et John BOWEN : Quantum error correcting codes in eigenstates of translation-invariant spin chains. *Physical Review Letters*, 123(11), Sep 2019.
- [49] Roy J. GLAUBER : Time-dependent statistics of the ising model. *Journal of mathematical physics*, 4(2):294, 1963.
- [50] Sergey BRAVYI et Barbara TERHAL : Complexity of stoquastic frustration-free hamiltonians. *Journal on Computing*, 39(4):24, 2009.
- [51] Sergey BRAVYI, David P. DIVINCENZO, Roberto OLIVEIRA et Barbara M. TERHAL : The complexity of stoquastic local hamiltonian problems. *Quantum Info. Comput.*, 8(5):361–385, mai 2008.
- [52] Milad MARVIAN, Daniel A. LIDAR et Itay HEN : On the computational complexity of curing non-stoquastic hamiltonians. *Nat. Commun*, 10(1571), 2019.
- [53] Lenart ZADNIK et Maurizio FAGOTTI : The Folded Spin-1/2 XXZ Model: I. Diagonalisation, Jamming, and Ground State Properties. *SciPost Phys. Core*, 4:10, 2021.
- [54] S. REDNER : One-dimensional ising chain with competing interactions: Exact results and connection with other statistical models. *J Stat Phys*, 25:15–23, 1981.
- [55] Hans BETHE : Zur theorie der metalle. eigenwerte und eigenfunktionen der linearen atomkette. *Zeitschrift für Physik*, 71(3):205–226, March 1931.

- [56] Michael KARBACH et Gerhard MÜLLER : Introduction to the bethe ansatz i. *Computers in Physics*, 11(1):36, Jan 1997.
- [57] Murray T. BATCHELOR : Bethe ansatz. *Encyclopedia of Mathematical Physics*, pages 253–257, 2006.
- [58] Jan MÖLTER, Thomas BARTHEL, Ulrich SCHOLLWÖCK et Vincenzo ALBA : Bound states and entanglement in the excited states of quantum spin chains. *Journal of Statistical Mechanics*, 2014(10):P10029, October 2014.
- [59] Jean HANUS : Bound states in the heisenberg ferromagnet. *Physical Review Letters*, 11(7):336–338, Oct 1963.
- [60] H. C. FOGEDBY : The spectrum of the continuous isotropic quantum heisenberg chain: quantum solitons as magnon bound states. *Journal of Physics C*, 13(9):L195–L200, Mar 1980.
- [61] Masanori KOHNO : Dynamically dominant excitations of string solutions in the spin-1/2 antiferromagnetic heisenberg chain in a magnetic field. *Physical Review Letters*, 102(3):037203, Jan 2009.
- [62] Martin GANAHL, Elias RABEL, Fabian H. L. ESSLER et H. G. EVERETZ : Observation of complex bound states in the spin-1/2 heisenberg XXZ chain using local quantum quenches. *Physical Review Letters*, 108(7):077206, Feb 2012.
- [63] E. HALLER, M. GUSTAVSSON, M. J. MARK, J. G. DANZL, R. HART, G. PUPILLO et H.-C. NAGERL : Realization of an excited, strongly correlated quantum gas phase. *Science*, 325(5945):1224–1227, Sep 2009.
- [64] Takeshi FUKUHARA, Peter SCHAUSS, Manuel ENDRES, Sebastian HILD, Marc CHENEAU, Immanuel BLOCH et Christian GROSS : Microscopic observation of magnon bound states and their dynamics. *Nature*, 502(7469):76–79, Sep 2013.
- [65] A. CEULEMANS, S. COJOCARU et L.F. CHIBOTARU : Finite size corrections within the continuum limit for quantum spins: two-magnon bound states in 1d heisenberg ferromagnet. *The European Physical Journal B*, 21(4):511–519, Jun 2001.
- [66] H.J. MIKESKA et A.K. KOLEZHUK : *Quantum Magnetism*, volume 645. Springer, 2004.
- [67] Michael WORTIS : Bound states of two spin waves in the heisenberg ferromagnet. *Physical Review*, 132(1):85–97, Oct 1963.
- [68] Ruber VERRESEN, Roderich MOESSNER et Frank POLLmann : Avoided quasiparticle decay from strong quantum interactions. *Nat. Phys.*, 15:750–753, 2019.
- [69] Noriaki SANOMIYA et Hosho KATSURA : Supersymmetry breaking and nambu-goldstone fermions in interacting majorana chains. *Physical Review D*, 99(4), Feb 2019.
- [70] Edward O'BRIEN et Paul FENDLEY : Lattice supersymmetry and order-disorder coexistence in the tricritical ising model. *Physical Review Letters*, 120(20), May 2018.
- [71] C. L. HENLEY : From classical to quantum dynamics at Rokhsar Kivelson points. *Journal of Physics Condensed Matter*, 16(11):S891–S898, mars 2004.
- [72] L. DELL'ANNA, O. SALBERGER, L. BARBIERO, A. TROMBETTONI et V. E. KOREPIN : Violation of cluster decomposition and absence of light cones in local integer and half-integer spin chains. , 94(15): 155140, octobre 2016.
- [73] Jonas RICHTER et Arijeet PAL : Anomalous hydrodynamics in a class of scarred frustration-free hamiltonians. *arXiv preprint arXiv:2107.13612*, 2021.
- [74] Stéphane VINET, Gabriel LONGPRÉ et William WITCZAK-KREMPA : Excitations and ergodicity of critical quantum spin chains from non-equilibrium classical dynamics. *arXiv preprint arXiv:2107.04615*, 2021.

- [75] Khagendra ADHIKARI et K. S. D. BEACH : Slow dynamics of the Fredkin spin chain. *arXiv:2011.07110 [cond-mat]*, novembre 2020. arXiv: 2011.07110.
- [76] Huw J WELLS : Quantum spin chains and random matrix theory. *arXiv preprint arXiv:1410.1666*, 2014.
- [77] Khagendra ADHIKARI et K. S. D. BEACH : Deforming the Fredkin spin chain away from its frustration-free point. *Physical Review B*, 99(5):054436, février 2019. Publisher: American Physical Society.
- [78] Khagendra ADHIKARI et K. S. D. BEACH : Tunable quantum spin chain with three-body interactions. *Physical Review B*, 102(18):184415, novembre 2020. Publisher: American Physical Society.

Annexe A

Annexe de l'article 1

A.1. Two-magnon continuum at large $|\kappa|$

It can be shown that the commutator of the Hamiltonian H in Eq. (1.2.7) and the Ising energy $H_{\text{Ising}} = \sum_i \sigma_i^z \sigma_{i+1}^z$ gives

$$[H, H_{\text{Ising}}] = 1 - \tanh^2 \kappa \quad (\text{A.1.1})$$

which is zero in the limit where $\kappa \rightarrow \pm\infty$. At $\beta = \infty$, this new conservation law strongly constrains the dynamics. For the two-magnon subsector, the interaction between the NN bound state and the continuum is also suppressed. In particular, we find that Eqs. (1.3.9,1.3.10) become

$$0 = Eg(1) \quad (\text{A.1.2})$$

$$3g(2) - \cos(K)g(3) = Eg(2) \quad (\text{A.1.3})$$

and thus we find a state ψ with $F(\text{NN},\psi) = 1$ and $E = 0$ at every value of K in Fig. A.1a. Similarly for $\kappa = -\infty$, $\delta_\kappa = 1$ and $\alpha_\kappa = -1$ and so Eqs. (1.3.9,1.3.10) now respectively become

$$2 = Eg(1) \quad (\text{A.1.4})$$

$$g(2) - \cos(K)g(3) = Eg(2) \quad (\text{A.1.5})$$

and we again find a state with $F(\text{NN},\psi) = 1$ but with $E = 2$ for every value of K in Fig. A.1b. The NNN branch in Fig. A.1b is the reflection of the one in Fig. A.1a about the $E = 2$ line.

A.2. Bloch basis

The common eigenstates of S_T^z and the translation operator T_1 are the Bloch states which are given by

$$|\vec{s}, k_m\rangle = \frac{1}{\sqrt{p}} \sum_{n=0}^{p-1} e^{i n k_m} (T_1)^{-n} |\vec{s}\rangle, \quad (\text{A.2.1})$$

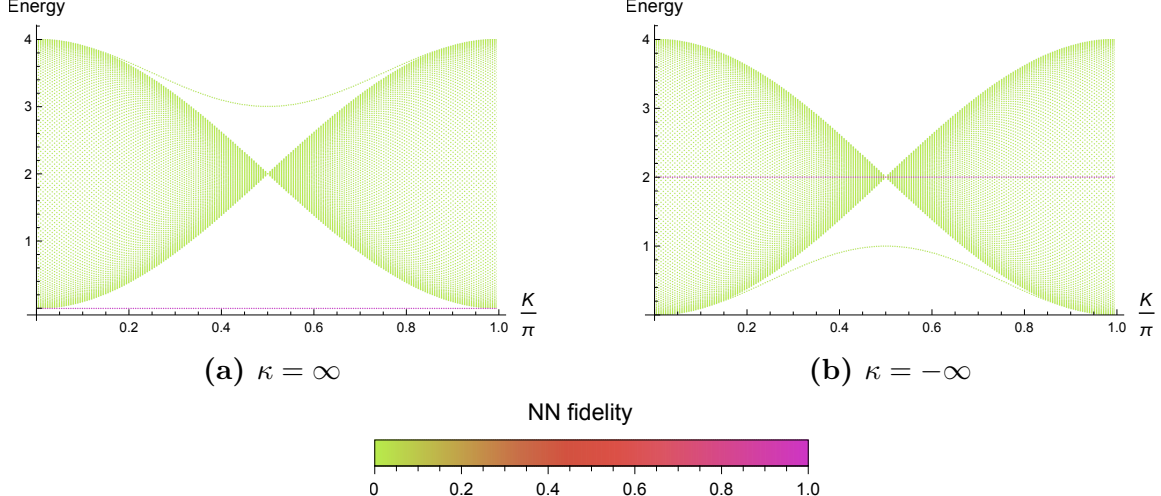


Fig. A.1. Two-magnon excitations and nearest neighbor fidelity for $N = 200$ and $\kappa = \pm\infty$ respectively in (a) and (b).

for $\vec{s} \in \{-1,1\}^N$ and $m \in \{0,1,\dots,N-1\}$ such that $p m/N \in \mathbb{N}$, where $k_m = 2\pi m/N$ is the momentum of the Bloch state and p is the period of the state $|\vec{s}\rangle$, i.e. the smallest integer $p > 0$ such that $T_1^p |\vec{s}\rangle = |\vec{s}\rangle$.

A.3. Numerical study of energy level spacings

Each state $|\vec{s}\rangle$ is stored as a binary number where each bit correspond to a site : 0 to \downarrow and 1 to \uparrow . For each orbit of T_1 we select the state \vec{s} with the lowest binary number as the representative of its Bloch state $|\vec{s},k\rangle$. To allow parallel computation of the Hamiltonian matrix elements and eigenvalues on a computer cluster, the basis states representatives are block-cyclically distributed using BLACS NUMROC function.

Because the action of the Pauli operators on the Bloch states are not straightforward, to compute the Hamiltonian elements in the Bloch basis we use the following simplification :

$$\langle \vec{s}',k | H | \vec{s},k \rangle = \left(\frac{1}{\sqrt{p'}} \sum_{n'=0}^{p'-1} e^{-i n' k} \langle \vec{s}' | T_{-n'}^\dagger \right) H \left(\frac{1}{\sqrt{p}} \sum_{n=0}^{p-1} e^{i n k} T_{-n} | \vec{s} \rangle \right) \quad (\text{A.3.1})$$

$$= \frac{1}{\sqrt{pp'}} \sum_{n'=0}^{p'-1} \sum_{n=0}^{p-1} e^{i(n-n')k} \langle \vec{s}' | T_{n'-n} H | \vec{s} \rangle \quad (\text{A.3.2})$$

$$= \frac{1}{\sqrt{pp'}} \sum_{n=1-p'}^{p-1} \min(p'+n, p-n, p', p) e^{i n k} \langle \vec{s}' | T_{-n} H | \vec{s} \rangle \quad (\text{A.3.3})$$

$$= \frac{1}{\sqrt{pp'}} \sum_{i=1}^N \sum_{n=1-p'}^{p-1} \min(p'+n, p-n, p', p) e^{i n k} \langle \vec{s}' | T_{-n} H_i | \vec{s} \rangle, \quad (\text{A.3.4})$$

where p and p' are the periods of the representatives \vec{s} and \vec{s}' , and

$$H_i = \gamma_\kappa \left(1 + \delta_\kappa \sigma_{i-1}^z \sigma_{i+2}^z\right) \left(\sigma_i^x \sigma_{i+1}^x + \sigma_i^y \sigma_{i+1}^y\right) + \frac{1}{4} \left[1 + \alpha_\kappa \sigma_i^z \sigma_{i+2}^z - (1 + \alpha_\kappa) \sigma_i^z \sigma_{i+1}^z\right]. \quad (\text{A.3.5})$$

To compute $\langle \vec{s}' | T_{-n} H_i | \vec{s} \rangle$ efficiently, bitwise operations on the binary numbers representing $|\vec{s}\rangle$ and $|\vec{s}'\rangle$ are used.

Finally, all the eigenvalues of the block-cyclically distributed Hamiltonian matrix are found using the PZHEEV subroutine from ScaLAPACK.

A.4. Finite-size scaling

As the chains get longer, the dimension of the sectors increases. Hence, the histogram of their level spacing distribution smoothens out and gets closer to the Wigner surmise. This can be seen in Fig. A.2 where we see how α decreases with N . It suggests that the distribution tends to the Wigner surmise in the $N \rightarrow \infty$ limit.

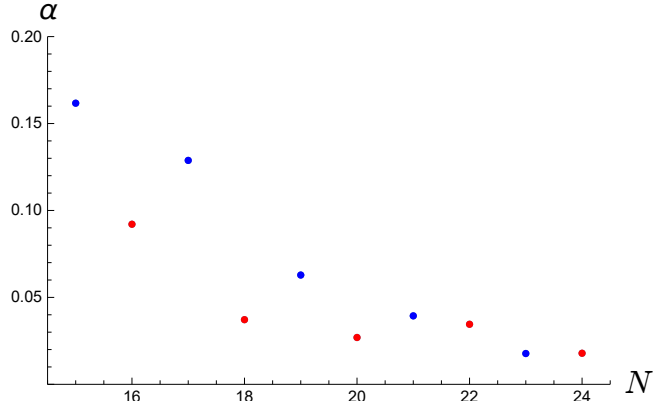


Fig. A.2. Fit coefficient α for increasing chain lengths N in the lowest strictly positive S_T^z and $k = 2\pi/N$ sectors. Blue dots have odd N and $S_T^z = 1/2$. Red dots have even N and $S_T^z = 1$.

Annexe B

Annexe de l'article 2

B.1. Finite-size effects on the dynamical exponents

The $z(N)$ values shown in Fig. 2.1b and 2.2b are obtained by using a power law fit on the triplets of points for chains of lengths $N - 1$, N and $N + 1$. The error bars on each point correspond to a confidence level of 90%. Dotted lines are the min and max slope lines that fit within these error bars. They are used to give a rough idea of the precision of the linear extrapolation.

B.2. Finite-size effects on the dispersion

From Fig. 2.4, we get values a_N and b_N from $N = 14$ to 23 . As seen in Fig. B.1a, a_N scales as a power law with an exponent $z_a = 1.4$. However, this value doesn't account for finite-size effects. The scaling of b_N rather seems to be linear in $1/N$ with different slopes for odd and even lengths, as seen in Fig. B.1b. In both cases, the exponent b_N approaches a value between 1.4 and 1.5 at $N \rightarrow \infty$.

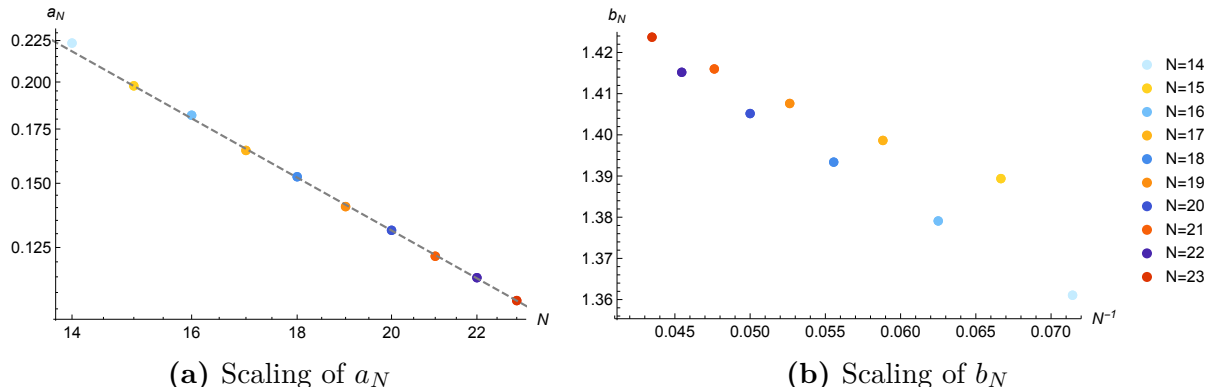


Fig. B.1. The scaling of the fit parameters a_N and b_N obtained from fits of the form $E = ak^b(\pi - k)^b$ in Fig. 2.4.